Challenge Journal of
CONCRETE RESEARCH LETTERS

Vol.15 No.1 (2024)

acoustic emission aerated concrete artificial neural network compressive strength corrosion cracking ductility durability energy absorption ferrocement flexural strength fly ash fracture mechanics mechanical properties mortar nanoparticle reinforced concrete self- compacting concrete steam curing strengthening superplasticizer tensile strength workability waste disposal water a tion

ISSN 2548-0928

TULPAR
ACADEMIC PUBLISHING

Challenge Journal of Concrete Research Letters

E-mail: *cjcrl@challengejournal.com*

Web page: *cjcrl.challengejournal.com*

Tulpar Academic Publishing
www.tulparpublishing.com

Challenge Journal of Concrete Research Letters

CONTENTS

Research Articles

TULPAR ACADEMIC PUBLISHING

Challenge Journal of Concrete Research Letters

Research Article

Reinforcement of concrete beams using waste carbon-nanoclay-fiberglass laminate pieces

Zinnur Çelik [a,*], Emrah Turan [b], Meral Oltulu [b], Gülşah Öner [c]

[a] *Department of Construction Technology, Pasinler Vocational School, Atatürk University, 25300 Erzurum, Türkiye*
[b] *Department of Civil Engineering, Atatürk University, 25240 Erzurum, Türkiye*
[c] *Department of Mechanical Engineering, Atatürk University, 25240 Erzurum, Türkiye*

ABSTRACT

In the last few decades, strengthening of structures in need of repair with fiber reinforced polymer (FRP) composite materials produced with different fiber types has gained great importance. Within the scope of this experimental study, the usability of hybrid glass and carbon composite laminates produced for different purposes and later cut into waste was investigated for concrete reinforcement. Hybrid composite laminates were produced in the form of glass-carbon-glass and carbon-glass-carbon, and the effect was investigated in two different sequences in the study. In addition, there are 3 different rates of nanoclay (0.50%, 0.75% and 1.25%) in the production of composite materials, and the effect of nanoclay ratio was investigated. In the study, two different numbers of composite laminates were adhered to the concrete samples produced in 70x70x280 mm dimensions and subjected to flexural strength test. In the Carbon-Glass-Carbon series using triple waste laminate pieces, the highest flexural strength was reported in the CGC-0.75-3 series, which achieved an increase of approximately 55% and 42% compared to the Control and Control-E series. It was determined that the effectiveness of the reinforcement technique of concrete with laminates in flexure did not change significantly depending on the number of laminate pieces. The main mode of failure in the experimental work was due to concrete fracture.

ARTICLE INFO

Article history:
Received 6 May 2023
Revised 10 July 2023
Accepted 26 July 2023

Keywords:
Waste laminate
Carbon-glass-carbon
Glass-carbon-glass
Flexural strength
Retrofitting

1. Introduction

In many existing structures, reinforced concrete structural elements become unable to meet the desired requirements during their service life due to design errors, increased loading, errors in the construction phase or dynamic loads such as wind, earthquake or environmental conditions that will cause aging, corrosion and deterioration (Obaidat et al. 2011; Askar et al. 2022; Hashemi 2011). It is a well-known fact that the insecurity of reinforced concrete structures made of low strength concrete and steel under the effect of dynamic loads. For these reasons, in most buildings that cannot meet the requirements, reinforcement is a more effective and economical solution instead of reconstruction. Reinforced beams can contribute to extending the service life of the structures and increasing the loading capacity, resulting in better performance of the structure (Ghobarah et al. 2002).

In the last century, traditional methods such as jacketing with concrete and steel plates have been used to strengthen reinforced concrete structures. However, one of these traditional methods used, while concrete jacketing increases the element sections and creates an excessive load on the structure, it has some disadvantages in terms of corrosion and application difficulties in steel jacketing (Askar et al. 2022; Raval and Dave 2013; Chalioris et al. 2014; Thermou et al. 2019; Shehata et al. 2009).

Due to the negative consequences of the above-mentioned strengthening methods, the reinforcement of

* *Corresponding author*. Tel.: +90-442-661-3982 ; E-mail address: zinnur.celik@atauni.edu.tr (Z. Çelik)
ISSN: 2548-0928 / DOI: https://doi.org/10.20528/cjcrl.2024.01.001

structural elements such as reinforced concrete beams with Fiber Reinforced Polymers (FRP) has increased significantly in recent years (Ascione and Feo 2000). The reason why FRP composites are preferred can be attributed to their higher performance due to their light weight, high hardness, corrosion resistance and ease of application (Amin et al. 2022a, 2022b; Talikoti and Kandekar 2019). FRP matrices are composite materials reinforced with different types of fibers. There are several types of FRPs: carbon FRP (CFRP), glass FRP (GFRP), basalt FRP (BFRP) and aramid FRP (AFRP). FRP composites are applied to reinforced concrete beams in the form of laminates, rods or fibers by bonding or mechanical anchoring (Hashemi 2011).

Miruthun et al. (2021) investigated the strengthening property of GFRP wrapped in three different ways in their study. The results showed that GFRP laminates improved the strength and ductility properties of the cracked RC beam. Obaidat et al. (2011) show that when beams strengthened using CFRP laminates are structurally efficient in shear and flexure.

In addition, ceramic, carbonaceous, clay, and polymer fillers are used in nano and micro sizes to improve the mechanical, impact and thermal properties of FRP composites (Sharma and Joshi 2023). Rafiq et al. (2017) found an increase of 23% and 11%, respectively, in the peak load and stiffness of the glass fiber reinforced epoxy composite with the addition of 1.5% nanoclay. Khan et al. (2011) showed that the addition of nanoclay to epoxy and CFRP improves the impact and flexural strengths of the composite. In Xu and Hoa (2008) stated that nanoclay added to carbon/epoxy composites in the amount of 2 phr increased the flexural strength by 38%. Öner et al. (2018) showed that the addition of nanoclay to hybrid carbon/fiberglass composites improves the flexural and tensile strength of the composite.

2. Research Significance

Recently, studies of strengthening concrete with glass and carbon fiber are widely seen in the literature. In this research, chopped waste materials consisting of epoxy matrix composite laminates prepared with these two fiber types were used to strengthen the concrete element. Composite materials used in reinforcement were not produced within the scope of this study, they are laminate pieces that were prepared for a different research and then became waste. With the increasing volume of waste, the rapid pollution of the environment poses a significant threat to biodiversity and human health. Consequently, there has been a surge in research efforts focused on waste recycling, both in terms of investigation and implementation (Şengel et al. 2022; Canbaz et al. 2021). Waste composite materials are arranged in two different ways as glass - carbon - glass (G-C-G) and carbon - glass - carbon (C-G-C). In addition, there are 3 different ratios of nanoclay in the content of composite materials. Hybrid waste material differs from concrete reinforcement studies in the literature in terms of both the regulation and use of nanoclay. Since the waste composite material is found in chopped form, its dimensions are smaller than the laminates in the literature. Therefore, the dimensions of the concrete flexural specimen were determined as 70x70x280 mm. The experimental study includes the application of 2 different number of composite laminate materials to the concrete sample using the bonding technique. As a result, the flexural strength of composite reinforced concrete was investigated.

3. Materials and Method

Within the scope of the experimental study, the cement type used in all mixtures is CEM I 42.5R Portland cement. The specific gravity and specific surface area of the cement were 3.12 g/cm^3 and 3486 cm^2/g, respectively. The chemical composition, physical and mechanical properties of cement is shown in Table 1. In the study, 4-25 mm coarse aggregate and 0-4 mm river sand were used as fine aggregate. The specific gravity of fine and coarse aggregates were 2.68 and 2.34, respectively.

Table 1. Chemical, physical and mechanical properties of cement.

Chemical Composition	%	Physical and Mechanical Properties	
SiO_2	19.17	Compressive strength 2 days (MPa)	27.2
Al_2O_3	4.50	Compressive strength 28 days (MPa)	55.6
Fe_2O_3	3.04	Specific surface area (Blaine) (cm^2/g)	3486
CaO	63.08	Specific gravity (g/cm^3)	3.12
MgO	1.78		
SO_3	2.89		
Insoluble materials	0.98		
Loss on ignition	3.93		
Na_2O	0.22		
K_2O	0.63		
Cl	0.0116		

In this study, laminates with Glass-Carbon-Glass and Carbon-Glass-Carbon sequences that were used by Öner et al. (2018) and Ünal et al. (2017) in their research and which were later disposed of were used. Carbon (245 g/m^2) and E-glass (200 g/m^2) fibers and a standard epoxy resin were used in the manufacture of the waste laminates. Nanoclay (0.50%, 0.75% and 1.25%) was added to the epoxy matrix by ultrasonic cavitation mixture. In the related study, the tensile and flexural strength range of the Carbon - Glass - Carbon composite series was determined as 550 MPa to 590 MPa and 908 MPa to 958 MPa, respectively. These range of the values were obtained as 599 MPa - 625 MPa and 794 MPa - 892 MPa for the Glass - Carbon - Glass sequence. The configuration of laminate materials (Carbon-Glass-Carbon) used by Öner et al. (2018) in their studies is presented in Fig. 1.

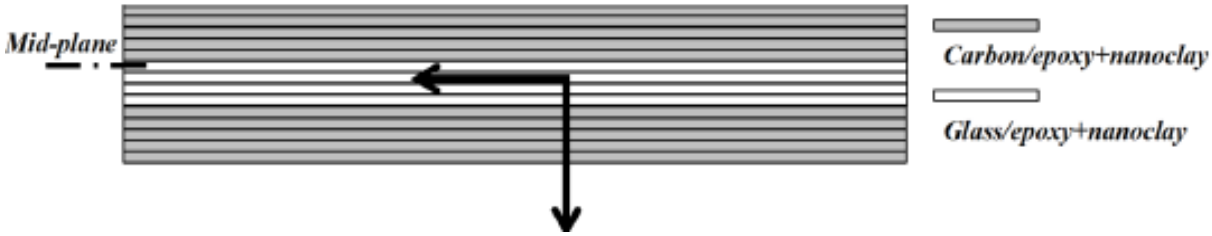

Fig. 1. Configuration of hybrid composite laminate (Öner et al. 2018).

The mixture composition by weight of the concrete used in this study is presented in Table 2. The strength of the concrete samples prepared in this study was aimed to be in the C40/50 class. The water-cement ratio was kept constant as 0.45 in all concrete samples and a 1.2% superplasticizer was used to obtain workability. These ratios were determined as a result of preliminary experiments.

Table 2. Amount of materials in 1 m^3 of concrete.

Materials	Amount (kg)
Cement	400.00
Water	181.40
Super Plasticizer	4.80
0-2 mm	510.26
2-4 mm	264.65
4-8 mm	331.14
8-16 mm	381.70
16-25 mm	165.94

In the study, 3x3x20 mm waste laminate pieces with G-C-G and C-G-C sequences were adhered to the midpoint of the 70x70x280 mm concrete beam samples with the help of epoxy. In addition, laminate pieces were tested by gluing them to the concrete beam in 2 different numbers (3 and 7). In order to ensure the surface contact of the beam with the epoxy, the beam surfaces are cleaned of dust and sawdust with the help of a compressor. It was applied to the epoxy surfaces with a roller to obtain a thickness of 0.8-1 mm. Laminates were adhered to the surface of the beams (Fig. 2).

Control and laminate reinforced 28-day beam samples were subjected to 3-point flexural test in accordance with TS EN 12390-5 (2010) standard. Each sample was named according to the arrangement, nanoclay ratio and number of laminates used. For example, in a CGC-0.50-3 code, the first three letters (CGC) represent the carbon-glass-carbon sequence, the number 0.50 represents the nanoclay ratio in the laminate, and 3 represents the number of laminate. In addition, only the epoxy bonded control group is symbolized as Control - E.

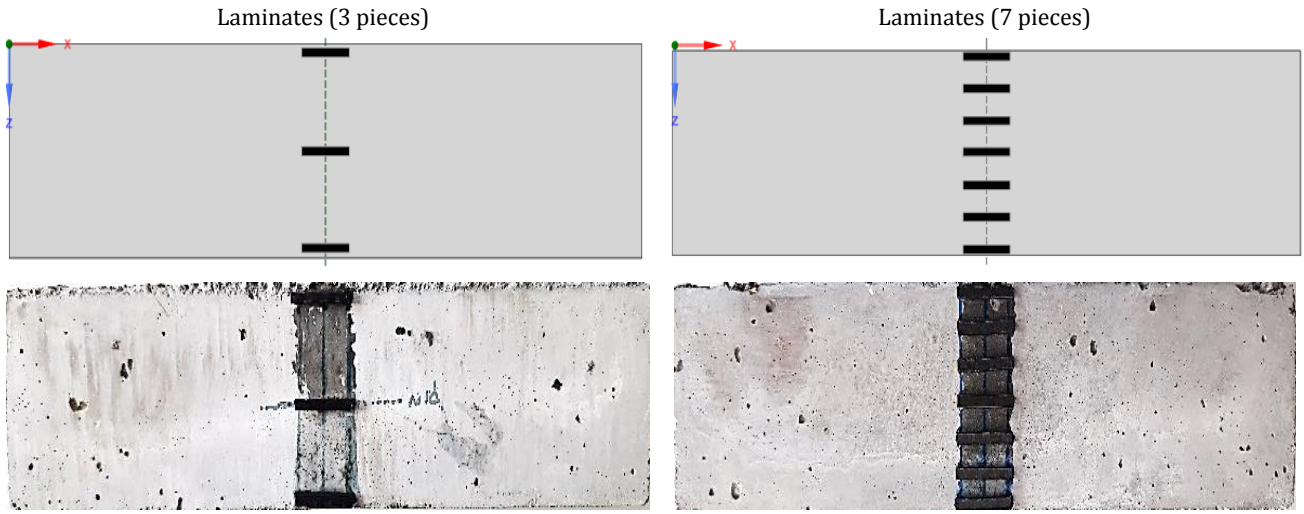

Fig. 2. Laminate-adhered concrete specimens.

4. Results and Discussion

4.1. Workability

The slump test on the concrete to which the laminate pieces were attached was carried out in accordance with TS EN 12350-2 (2010). The slump value of the produced concrete was determined as 18.8 cm. This value provided the S4 class values, one of the consistency classes given in the TS EN 206-1 (2021) standard.

4.2. Flexural strength

The flexural strength results of concrete reinforced with 3 and 7 pieces of Carbon-Glass-Carbon laminate are given in Fig. 3. The mean values for flexural strength of concrete to the series without nanoclay were published in previous study by Turan et al. (2023).

When Fig. 3 is examined, the lowest flexural strength value was obtained from the control sample with 5.59 MPa. An increase of 9.12% was observed in the flexural strength of the Control-E series, which was produced by adhering only epoxy to the control sample, compared to the control sample. The highest flexural strength in the triple array Carbon-Glass-Carbon series was obtained from the CGC-0.75-3 group with a value of 8.69 MPa. This value was 55.46% and 42.46% higher compared to the Control and Control-E sample, respectively. The flexural strength of CGC-0.75-3 and CGC-1.25-3 groups of Carbon-Glass-Carbon series with nano clay added was higher than the series without nano clay (CGC-0) addition. In the C-G-C series with nanoclay reinforced with three pieces of laminate, the highest concrete flexural strength was calculated in the group with 0.75% nanoclay. Obaidat et al. (2011) used CFRP laminates to retrofitting reinforced concrete beams in their study. The increase in the maximum load of shear force and flexural strength of the laminate reinforced samples reached values between approximately 23% and 33%, respectively.

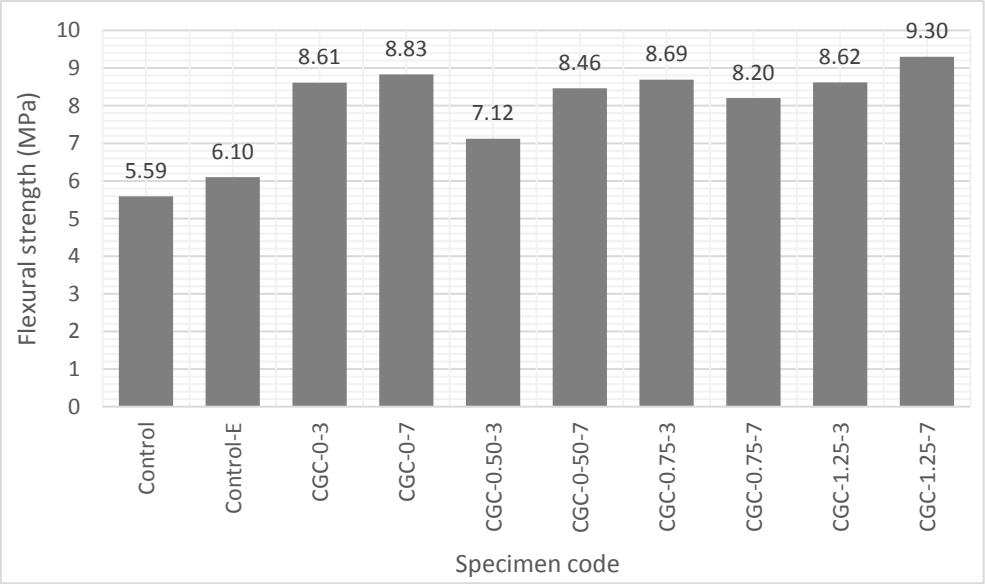

Fig. 3. Flexural strength of concrete reinforced with 3 and 7 pieces of CGC laminate.

In the CGC series with 7 laminate pieces, the highest concrete flexural strength value was obtained from the CGC-1.25 series with 9.30 MPa. This value was 66.36% and 52.46% higher than the flexural strength of the Control and Control-E series, respectively. It was determined that the flexural strength of CGC-0-7, CGC-0.50-7 and CGC-0.75-7 series increased by 44.75%, 38.68% and 34.42%, respectively, compared to the Control-E sample.

The flexural strength results of concrete reinforced with 3 and 7 pieces of Glass-Carbon-Glass laminate are given in Fig. 4. The flexural strength values of the Glass-Carbon-Glass series reinforced with 3 laminates were calculated in the range of 8.08 MPa - 8.84 MPa. The highest flexural strength in the triple array Glass-Carbon-Glass group was obtained in the GCG-0.75-3 series with 8.84 MPa. This value detected in the GCG-0.75-3 series was 58.14% and 44.92% higher compared to the Control and Control-E groups, respectively. The flexural strength of the series containing 0.50%, 0.75% and 1.25% nanoclay was determined to increase by 6.43%, 9.40% and 8.17%, respectively, compared to the GCG-0-3 series without nanoclay.

The flexural strength values of the 7-arrays Glass-Carbon-Glass series were calculated in the range of 8.45 MPa - 9.09 MPa. The highest flexural strength value was obtained from the GCG-0.75-7 series with an increase of 49.02% compared to the Control-E series. Compared to the flexural strength of the Control-E sample, an increase of 40.32% and 42.62% was detected in the GCG-0-7 and GCG-0.50-7 series, respectively. Although the flexural strength of the 1.25% nanoclay-containing GCG series decreased, it was 38.52% higher than the Control-E series. In the GCG-0.50-7 and GCG-0.75-7 series, 1.63% and 6.19% increase in flexural strengths were reported compared to GCG-0-7, respectively.

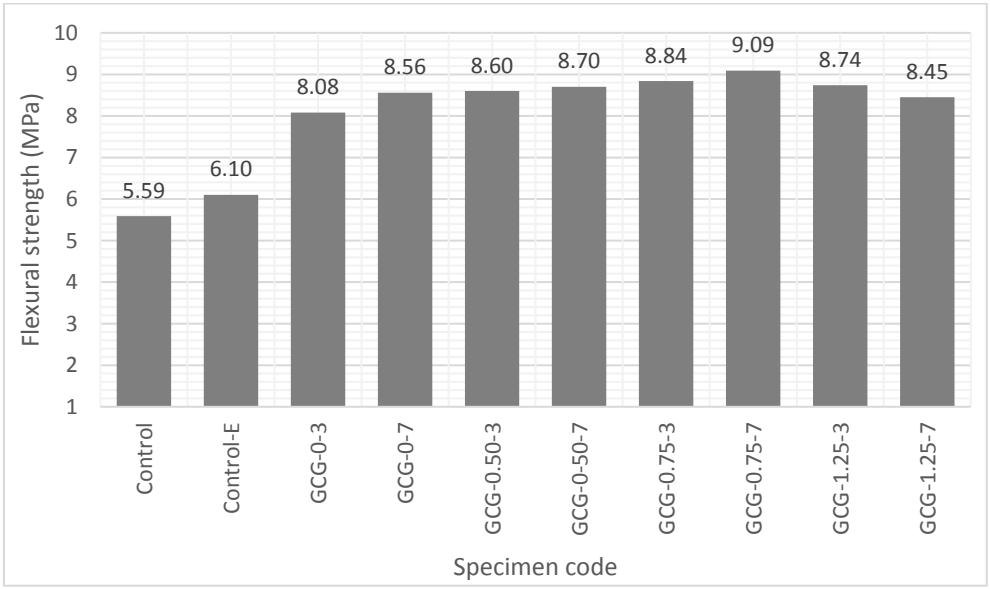

Fig. 4. Flexural strength of concrete reinforced with 3 and 7 pieces of GCG laminate.

As a result of examining together the CGC and GCG series used in triples, the highest flexural strength values in nanoclay added samples were obtained from the GCG series. In addition, the optimum value in terms of nano clay was determined as 0.75% in both arrays (CGC-GCG) strengthened with 3 pieces of laminate, and the addition of 1.25% nanoclay decreased the flexural strength in both groups. This is attributed to the increase in the viscosity of the epoxy and the amount of air bubbles during the mixing process due to the increased amount of nanoclay used (Xu and Hoa 2008). These results are similar to the tensile and flexural strength results of the laminates in the Öner et al study, where the waste material was obtained. Hosny et al. (2006) determined that the ultimate carrying capacity of reinforced concrete beams strengthening with hybrid GFRP and CFRP laminates increased by 27.2% compared to the control sample.

Increasing the number of laminate pieces adhered to the beams from 3 to 7 resulted in an increase in flexural strength of approximately 1.1% to 7.8%, except for the CGC-0.50 series. This is an indication that the number of laminate pieces attached to the concrete is not an important parameter in increasing the flexural strength. Because the results showed that the main failure mode was concrete, not laminate pieces, which increased the effectiveness of the reinforcement (Fig. 5).

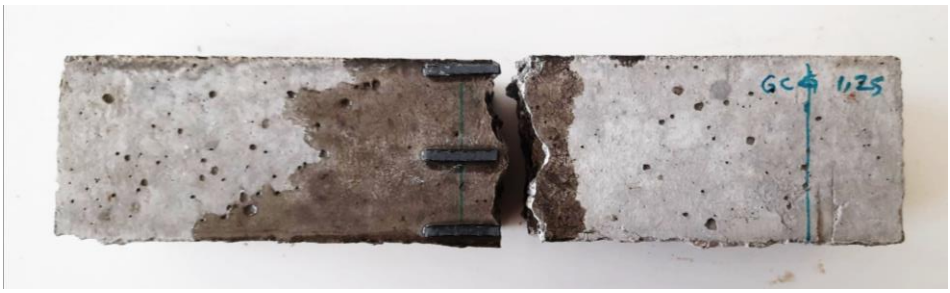

Fig. 5. Fracture mode of concrete reinforced with laminate pieces.

5. Conclusions

This study aims to investigate the effect of different numbers of laminated pieces of carbon-Glass-Carbon and Glass-Carbon-Glass arrays with different ratios of nanoclay in the waste state on the flexural strength of concrete. The main conclusions can be summarized as follows:

- In the Carbon-Glass-Carbon series using triple waste laminate pieces, the highest flexural strength was reported in the CGC-0.75-3 series, which achieved an increase of approximately 55% and 42% compared to the Control and Control-E series.
- The highest flexural strength in the triple array Glass-Carbon-Glass group was obtained in the GCG-0.75 series with 8.84 MPa. In addition, in the triple use of both arrays (CGC-GCG), the highest value in terms of flexural strength of concrete was obtained in the samples using 0.75% nano clay.
- It was determined that the use of laminate pieces with 7 in the CGC-0, CGC-0.50 and CGC-0.75 series increased the flexural strength of concrete by 44.75%, 38.68% and 34.42%, respectively, compared to the Control-E sample.
- It was determined that when the 7-arrays GCG waste laminate pieces used in the reinforcement of concrete

contained 0.50% and 0.75% nanoclay, the flexural strength of the concrete increased by 1.63% and 6.19%, respectively, compared to GCG-0.

- Increasing the number of laminate pieces adhered to concrete beams from 3 to 7 resulted in an increase in the flexural strength of concrete by approximately 1.1% to 7.8%, excluding the CGC-0.50 series. The fact that the numerical increase in the laminate pieces does not cause a significant increase in the flexural strength results is due to the fact that the main failure mode in the samples is in the concrete, not the laminate pieces, which increases the efficiency of the reinforcement.
- Since the laminate parts used in this study were waste, there was no alternative for the dimensions of the parts. In future studies, it is thought that if the laminate pieces used in this study are used in larger sizes, it may be more effective in repair and reinforcement of concrete. In addition, the use of laminate parts in the reinforcement of reinforced concrete samples, which will show more ductile behavior, can provide better observation of the behavior of laminates.

Acknowledgements

None declared.

Funding

The authors received no financial support for the research, authorship, and/or publication of this manuscript.

Conflict of Interest

The authors declared no potential conflicts of interest with respect to the research, authorship, and/or publication of this manuscript.

Author Contributions

All of the authors made substantial contributions to conception and design, or acquisition of data, or analysis and interpretation of data; were involved in drafting the manuscript or revising it critically for important intellectual content; and gave final approval of the version to be published.

Data Availability

The datasets created and/or analyzed during the current study are not publicly available, but are available from the corresponding author upon reasonable request.

REFERENCES

Amin MN, Salami BA, Zahid M, Iqbal M, Khan K, Abu-Arab AM, Alabdullah AA, Jalal FE (2022a). Investigating the bond strength of FRP laminates with concrete using LIGHT GBM and SHAPASH analysis. *Polymers*, 14(21), 4717.

Amin MN, Iqbal M, Jamal A, Ullah S, Khan K, Abu-Arab AM, Al-Ahmad QMS, Khan S (2022b). Gep tree-based prediction model for interfacial bond strength of externally bonded FRP laminates on grooves with concrete prism. *Polymers*, 14(10), 2016.

Ascione L, Feo L (2000). Modeling of composite/concrete interface of RC beams strengthened with composite laminates. *Composites Part B: Engineering*, 31(6-7), 535-540.

Askar MK, Hassan AF, Al-Kamaki YSS (2022). Flexural and shear strengthening of reinforced concrete beams using FRP composites: A state of the art. *Case Studies in Construction Materials*, 17, e01189.

Canbaz M, Kara İ, Topçu İ (2021). Effect of high temperature on the mechanical behavior of cement-bonded wood composite produced with wood waste. *Challenge Journal of Structural Mechanics*, 7(1), 42-48.

Chalioris CE, Thermou GE, Pantazopoulou SJ (2014). Behaviour of rehabilitated RC beams with self-compacting concrete jacketing–Analytical model and test results. *Construction and Building Materials*, 55, 257-273.

Ghobarah A, Ghorbel MN, Chidiac SE (2002). Upgrading torsional resistance of reinforced concrete beams using fiber-reinforced polymer. *Journal of Composites for Construction*, 6(4), 257-263.

Hashemi S (2011). Strengthening of concrete structures using carbon fibre reinforced polymers and cement-based adhesives. *Ph.D. thesis*, Monash University, Clayton, Victoria, Australia.

Hosny A, Shaheen H, Abdelrahman A, Elafandy T (2006). Performance of reinforced concrete beams strengthened by hybrid FRP laminates. *Cement and Concrete Composites*, 28(10), 906-913.

Khan SU, Iqbal K, Munir A, Kim JK (2011). Quasi-static and impact fracture behaviors of CFRPs with nanoclay-filled epoxy matrix. *Composites Part A: Applied Science and Manufacturing*, 42(3), 253-264.

Miruthun G, Vivek D, Remya PR, Elango KS, Saravanakumar R, Venkatraman S (2021). Experimental investigation on strengthening of reinforced concrete beams using GFRP laminates. *Materials Today: Proceedings*, 37, 2744-2748.

Obaidat YT, Heyden S, Dahlblom O, Abu-Farsakh G, Abdel-Jawad Y (2011). Retrofitting of reinforced concrete beams using composite laminates. *Construction and Building Materials,* 25(2), 591-597.

Oner G, Unal HY, Pekbey Y (2018). Mechanical performance of hybrid carbon/fiberglass composite laminates reinforced with nanoclay. *Acta Physica Polonica A*, 134, 164-167.

Rafiq A, Merah N, Boukhili R, Al-Qadhi M (2017). Impact resistance of hybrid glass fiber reinforced epoxy/nanoclay composite. *Polymer Testing*, 57, 1-11.

Raval SS, Dave UV (2013). Effectiveness of various methods of jacketing for RC beams. *Procedia Engineering*, 51, 230-239.

Sharma A, Joshi SC (2023). Enhancement in fatigue performance of FRP composites with various fillers: A review. *Composite Structures*, 116724.

Shehata IAEM, Shehata LCD, Santos EWF, Simoes MLF (2009). Strengthening of reinforced concrete beams in flexure by partial jacketing. *Materials and Structures*, 42, 495-504.

Şengel H, Kınık K, Erol H, Canbaz M (2022). Effect of waste steel tire wired concrete on the mechanical behavior under impact loading. *Challenge Journal of Structural Mechanics*, 8(4), 150-158.

Talikoti RS, Kandekar SB (2019). Strength and durability study of concrete structures using aramid-fiber-reinforced polymer. *Fibers*, 7(2), 11.

Thermou GE, Papanikolaou VK, Lioupis C, Hajirasouliha I (2019). Steel-reinforced grout (SRG) strengthening of shear-critical RC beams. *Construction and Building Materials*, 216, 68-83.

TS EN 206 (2021). Concrete - Specification, performance, production and conformity. Turkish Standards Institute, TSE, Ankara, Türkiye.

TS EN 12350-2 (2010). Testing fresh concrete-Part 2: Slump test. Turkish Standards Institute, TSE, Ankara, Türkiye.

TS EN 12390-5 (2010). Testing hardened concrete-Part 5: Flexural strength of test specimens. Turkish Standards Institute, TSE, Ankara, Türkiye.

Turan E, Oltulu M, Yıldız İ, Çelik Z, Öner G (2023). The use of waste carbon/fiber glass reinforced laminates on the strengthening of concrete beams. *4. International Hasankeyf Scientific Research and Innovation Congress*, Batman, Türkiye.

Ünal HY, Öner G, Pekbey Y (2017). Comparison of the experimental mechanical properties and DMA measurement of nanoclay hybrid composites. *European Mechanical Science*, 2(1), 31-36.

Xu Y, Van Hoa S (2008). Mechanical properties of carbon fiber reinforced epoxy/clay nanocomposites. *Composites Science and Technology*, 68(3-4), 854-861.

Challenge Journal of Concrete Research Letters

Research Article

Advantageous approach for boron ores used in cement production: optimization of dehydration

Mustafa Engin Kocadağistan [a,*], Harun Arslan [a]

[a] *Department of Metallurgy and Material Engineering, Atatürk University, 25240 Erzurum, Türkiye*

ABSTRACT

Boron with a certain water content is used for industrial purposes, including cement production. It is necessary to perform and optimize heat treatments and determine the water content. The heat treatment is applied to boron ores that must be used for cement production. However, these processes take time and increase costs. With this study, it will be possible to obtain boron products with the desired properties in a shorter time by determining the optimal parameters for dewatering processes. Colemanite and ulexite ores were reduced to a grain size of 44 microns by ore dressing processes and subjected to dewatering. The Taguchi method was used to optimize the dehydration of colemanite and ulexite ores. The orthogonal design of experiments method $L_{18}(6^1 3^2)$ 3 factors, 18 trials was chosen to determine the design of experiments. The changes in the H_2O-CaO-Na_2O-B_2O_3 concentrations were determined on the basis of the analyses performed. TG/DTA analyses were carried out for comparison with the dehydration processes. In the optimization processes performed using the Taguchi method, the maximum water removal was achieved with 1 g of ore and a period of 6 hours. H_2O removal was 98.42% at 650 °C for colemanite and 99.1% at 300 °C for ulexite. It has been shown that the dehydration of ulexite and colemanite ores can be optimized and the boron product with the desired properties can be obtained in a short time, which is an advantage for its use in the cement industry. It is expected that this study will serve as an important basis for future applications of B_2O_3 cement.

ARTICLE INFO

Article history:
Received 6 November 2023
Revised 9 January 2024
Accepted 19 January 2024

Keywords:
Colemanite
Ulexite
Dehydration
Optimization
Taguchi method

1. Introduction

Boron ores are commonly known as borates and borosilicates. They are always associated with oxygen in mineral deposits (Helvacı 2015). They generally contain B_2O_3. They gain value depending on the amount of crystal water (H_2O) (Helvacı 2017; Çelik et al. 1994; Tunç et al. 1997; Şener et al. 2000). The most commonly used species in the industry are borax, colemanite and ulexite. Colemanite; among boron minerals, it is the most abundant type. It contains Ca, is transparent, colorless, and occurs in the form of crystals. Its density is 2.42 g/cm^3 and its hardness is 4.0-4.5 on the Mohs hardness scale (DPT 2001). It dissolves very poorly in water, but can easily dissolve in acid and acid salts (Akyıldız 2012). In Türkiye, it is concentrated in some regions of Balıkesir, Kütahya, Bursa, and Eskişehir (Ulusoy 2012). Chemical formula: ($2CaO.3\ B_2O_3.5H_2O$) and its B_2O_3 content is 50.8%. Ulexite; It is generally found in the form of soft, highly moist, and fibrous crystals. The hardness is 2.5 and the specific gravity is 1.955 g/cm^3. Its chemical composition is ($Na_2O.2CaO.5\ B_2O_3.16H_2O$) and in pure form, it contains 42-43% B_2O_3 (Çelik 2007).

Boron products are light, resistant to stress and chemical effects, and are mostly used in the chemical and cosmetic industries, photography, paint, leather, and cement industries (Topçu and Soyhan 2022; Kurtuluş and Kurtuluş 2021). Anhydrous boron (B_2O_3) has been used in cement production for many years. Research has shown that cement made with anhydrous (pure) B_2O_3

* *Corresponding author*. Tel.: +90-442-231-6036 ; E-mail address: mengink@atauni.edu.tr (M. E. Kocadağistan)
ISSN: 2548-0928 / DOI: https://doi.org/10.20528/cjcrl.2024.01.002

significantly improves its properties (Demirel and Nasıroğlu 2017). In one study, mixed cement was made by adding boron waste with the same B_2O_3 content to the cement in varying proportions. Strength and durability tests were conducted with these cements. It was found that the mineral additives used in cement production not only have a positive impact on the environment but also have a positive impact on costs by saving natural raw materials and energy. These studies are important in order to recycle industrial waste in various sectors, eliminate environmental problems, and contribute to the country's economy. It is obvious that boron minerals and waste are suitable for cement production in the world, especially in our country. The use of boron minerals and wastes, which do not have negative effects on cement properties and do not contain harmful components, offers great advantages in cement production (Eyyüboğlu 2013; Oruç et al. 2004). In particular, the studies carried out jointly by Boren National Boron Research Institute and Turkish Cement Manufacturers Association (TÇMB) and industrial scale cement production in Denizli and Göltaş cement factories are one of these studies (Demirel and Nasıroğlu 2017). In their study, Elbeyli et al. (2003) added "boral gypsum" produced during the manufacture of colemanite (heat treated) to Portland cement and investigated its effects on mechanical properties. TGA, XRD, and gradual heating were applied as heat treatments. Boron was added to Portland cement at the clinker stage in an amount of 5-7% of the cement weight and subjected to heat treatment. Gradual heating was carried out at a rate of 10 °C/min up to 500 °C. At the end of the experiments, no change in strength was observed in the non-heat-treated (5%) specimens with boral gypsum addition, while the strength of the heat-treated (5%) specimens with boral gypsum addition increased by 25%. Pehlivanoğlu et al. (2013) investigated the effects of boron compounds on the setting time of Portland cement, boron-active belite cement, and calcium aluminate types of cement. Boric acid was added to these cement samples at a dosage of 0.25% and 1%. It was found that despite the increase in the amount of boric acid, the initial and final setting times also increased.

In another study in which colemanite and ulexite minerals were added to mortar samples, unheated and heat-treated colemanite minerals were added separately to the mortar. The minerals were subjected to heat treatment at 150 °C-24 hours and 600 °C-6 hours. In this study conducted by Şener et al. (2000), it was observed that the minerals completely lost their moisture at 150 °C. It was found that the prolongation of setting times by heat treatments at 150 °C and 600 °C further increased for the colemanite mineral. For this reason, heat treatment may be considered appropriate in cases where a longer setting time is required at lower additive rates (Durmuş 2016). The results of the setting time tests in this study are consistent with the results of the studies by Olgun et al. (2006) and Pehlivanoğlu et al. (2013), which state that boron additives increase the setting times. Based on the results of the bending and compression tests of heat-treated specimens with colemanite additive, it was found that the heat-treated colemanite mineral has no effect on mechanical strength.

The use of boron minerals and boron waste in cement has become a very important issue in recent years. In cement production, the use of boron increases the durability of concrete. Boron cement is especially preferred in the construction of concrete roads and dams. In order to investigate the usability of boron cement in concrete road construction and its effect on the performance of the road, a 1600 m long concrete road was constructed, 1000 m of which was located in the Black Sea region (Yenialaca 2009). The use of boron in cement production is not a new practice. Considerable improvements have been observed in the properties of cement produced using pure B2O3. With this in mind, appropriate studies have been initiated in our country and it has been determined that colemanite may be the most suitable mineral. When colemanite, a boron mineral, is used in cement production at the rate of 8%, it lowers the burning temperature of the clinker and improves the properties of the cement (Eyyüboğlu 2013). Boron cement; shows better properties than Portland cement in terms of parameters such as strength, water and gas permeability, and heat of hydration. Low heat of hydration significantly reduces cooling requirements, especially for mass concrete. Calcium borates are very useful plasticizers, as they reduce the viscosity and surface tension of the melt in the rotary kiln during cement production (Boren 2016).

In order for boron ores to be used in industry, they must undergo certain processes such as crushing, grinding, and dewatering, and the water of crystal in their structure must be removed. Calcination/dehydration processes must be applied to remove the crystal water bound in their structure (Kılcı 2011). As can be seen, boron ores are offered for industrial use by removing the chemically bound water they contain through calcination or dehydration processes (Kayandan et al. 2004). The main purpose of dehydration of boron minerals is to prepare the ores for commercial use, i.e., to give them a higher useful and economic value by releasing the crystal water they contain (Tunç et al. 2001; Şener et al. 2000). Thus, calcined boron ores can be used in many industries. Şener and Ozbayoğlu (1994) conducted a study on the calcination processes of ulexite and colemanite minerals (which are endothermic). In this study, they mixed colemanite and ulexite and calcined them at 400-450 °C for half an hour. They found that the colemanite ore crumbled and dissolved, while the ulexite ore did not break and turned into a porous, hard structure.

In addition to the dehydration processes, which are important for the use of boron ores in industrial applications, some optimization processes can also be carried out for these heat treatments, which bring both time and economic benefits. One of these methods is the Taguchi method. The general idea of the Taguchi method is to fit small factorial or orthogonal arrangements of experimentally calculated elements to assembly variations and to perform estimated calculations. This method can be applied to all open or closed functions (Samtaş and Gülesin 2005). The Taguchi method is an experimental design method that attempts to minimize product and process variability by selecting the most appropriate combination of levels of controllable factors versus the uncontrollable factors that cause product and process variabil-

ity (Baynal 2005). Applying parameter design in the Taguchi method to optimize a process with multiple performance characteristics involves the following steps: the determination and calculation of performance characteristics and the selection of process parameters that can be evaluated, the provision of the number of parameter levels for the process and the interaction between possible process parameters, the selection of the appropriate orthogonal arrangement, the determination of process parameters in the orthogonal arrangement, the management of experiments based on the arrangement of the orthogonal arrangement, analysis of experimental results using ANOVA and performance characteristics, selection of optimal process parameters, verification of optimal process parameters (with all verification experiments) (Çopur et al. 2004; Kocadağistan 2007). The Taguchi method occupies a very important place in the technological and scientific development of quality and has brought a completely different perspective to the definition of quality (Kumsal 1994). In a study, the formation of calcium carbide slag by the Taguchi method and its use in the production of CaO briquettes by calcination processes was investigated. In this study, since the disposal of calcium carbide slag (CCS), obtained as a by-product during the Acetylene gas process, poses an environmental problem, it is aimed to use CCS in the preparation of calcium oxide (CaO) briquettes for reuse in calcium carbide production. As parameters; binder types (phosphoric acid (H_3PO_4), molasses, and corn syrup), binder amount (1, 3, and 5%), briquette pressure (20, 28, and 36 MPa), calcination temperature (800, 900, and 1000 °C), and calcination time (30, 45, and 60 min.) was selected. The effect of these parameters on the strength of the CaO briquettes was examined using the Taguchi approach (Altıner 2018). In another study, the optimization of the dissolution of calcined colemanite mineral in methyl alcohol by CO_2 in the autoclave system was investigated using the Taguchi method. In the study, the process of optimizing the dissolution of colemanite ore in methyl alcohol with CO_2 in a high-pressure reactor was evaluated using the Taguchi method (Kızılca and Çopur 2017).

2. Materials and Method

2.1. Materials

In the experiments, colemanite and ulexite ores obtained from Etibank Bor mines were used (Fig. 1). Chemical analysis results of colemanite and ulexite ores are given in Table 1.

Table 1. Analysis results of colemanite and ulexite ores.

Compound	Colemanite	Ulexite
	%	%
B_2O_3	50.97	43.1
CaO	27.18	13.8
Na_2O	-	7.6
H_2O	21.85	35.4

Fig. 1. Ulexite and colemanite ore samples.

Laboratory-type jaw crusher, ball mill, and mechanical sieve were used in ore size reduction processes. In the sieving process, 60 mesh (283 micron/0.28 mmx0.28 mm mesh size, 60 mesh, 0.14 mm wire diameter, 23.62 mm/number of holes) and 325 mesh (43 micron/0.043 mmx0.043 mm mesh size, 325 mesh, 0.035 mm Standard sieves with dimensions (wire diameter, 127.952 mm/number of holes) were used. A muffle furnace (Nabertherm, Germany) with a maximum temperature of 1100 °C was used for dehydration experiments. TG analyses were performed with differential thermal analysis and thermogravimetric analyzer (DTA-TG system, SETARAM Labsys 3.0). Other materials; 35 mL porcelain crucible, desiccator, OHAUS-PA214C brand precision balance, and other experimental materials.

2.2. Method

In the sample preparation process of ulexite and colemanite ore for dehydration experiments, a 500 g sample

was taken by cone and quartering method and was first crushed to 60 mesh (250 micron) size in a jaw crusher, and then ground to 325 mesh (45 microns) size in a ball mill. Approximately 200 g ore samples to be used in the experiments were sieved using a mechanical sieve and the samples were made ready for dehydration processes. In the Taguchi method, the experimental design was planned first. The problem was defined, performance characteristics were determined, and the design was realized. Parameter design is carried out in order to determine the factors and levels that affect the target value of the performance characteristic and make this optimum. There are two stages in parameter design; robust design and orthogonal arrays. Robust design is an optimization method applied to introduce new technologies in the design of products and processes (Taguchi et al. 1999; Şanyılmaz 2006). After the robust design, an orthogonal array selection was made, which determines how all experimental combinations will be carried out. Thus, fewer experiments were performed with a larger number of factors (Özden 2020; Mercan 2019). The values used in the experiments were converted to S/N (signal/noise) ratios and analysis of variance (ANOVA) was performed (Danışman and Yalçındağ 2023). In order to verify the optimal factor levels determined by the Taguchi method, a confidence interval was created for the average response value under optimal conditions (Yılmaz and Keskin 2019). Dehydration experiments were carried out to verify the data found in the experiments performed with the Taguchi method. In order to determine the experimental plan in the optimization studies of the dehydration of colemanite and ulexite ores (Taguchi method), orthogonal layout experimental design method $L_{18}(6^1 3^2)$ 3 factors, 18 experiments were selected. In optimization experiments, dehydration temperature, dehydration time, and ore amount were selected as experimental parameters. The data obtained as a result of the experiments were evaluated according to Eq. (1) for each level of each parameter and performance criteria were calculated.

$$\text{Smaller – better } S/N_S = -10log\left(\frac{1}{n}\sum_{i=1}^{n} y_i^2\right) \quad (1)$$

For the dehydration temperature of ulexite ore, 300 °C was chosen in the parameter levels, and it was aimed to obtain precise data against the possibility of variations in weight differences at temperatures of 350 and above. The parameters used in the optimization experiments are arranged as given in Table 2.

In the dehydration process, the temperature of the furnace was adjusted according to the determined parameters and the weighed colemanite and ulexite ores were placed in porcelain crucibles and placed in the furnace. Each sample, whose dehydration process was completed, was left to cool in the desiccator together with the crucible to prevent moisture, was weighed and the weight differences were recorded. TG analyzes were performed with differential thermal analysis and thermogravimetric analyzer (DTA-TG system, SETARAM Labsys 3.0). Analyzes were performed using an aluminum oxide crucible at a heating rate of 10 °C/min. The process flow diagram of the working method is given in Fig. 2.

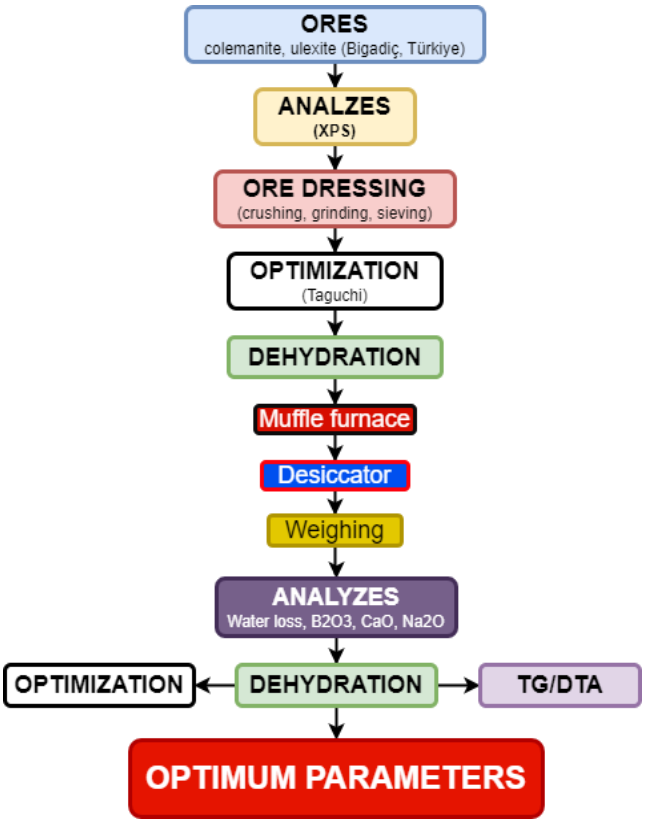

Fig. 2. Process flow diagram.

Table 2. Parameters used in optimization of dehydration of colemanite and ulexite ores.

Ore	Parameters	Level					
		1	2	3	4	5	6
Colemanite	Dehydration temperature (°C)	400	450	500	550	600	650
	Dehydration time (h)	2	4	6	-	-	-
	Amount of ore (g)	1	3	5	-	-	-
Ulexite	Dehydration temperature (°C)	50	100	150	200	250	300
	Dehydration time (h)	2	4	6	-	-	-
	Amount of ore (g)	1	3	5	-	-	-

3. Results and Discussion

3.1. Optimization of the dehydration process of colemanite and ulexite ores

The parameters selected for the optimization of dehydration processes to be applied to colemanite and ulexite ores and the water concentrations in the ores at the end of the experiments are given in Table 3. After the experimental groups determined according to the Taguchi method were completed, dehydration experiments were carried out to verify the data obtained and compared with these data.

Figs. 3 and 4 were prepared by considering the results calculated for both ores as the y-axis and the levels of the parameters as the x-axis. The first part in Figs. 3 and 4 shows the temperature levels, the second part shows the time levels and the third part shows the ore amount levels. Considering the S/N_s ratio, the point where the performance criterion has the lowest value indicates the best level of the relevant parameter. When the test results are examined, the parameter values that give the best results for colemanite ore using the Taguchi method are; 650 °C temperature, 6 h time, and 1g ore amount. For ulexite ore, the parameter values that give the best results; it is 300 °C temperature, 6 h time, and 1g ore amount. Since the obtained levels were not included in the $L_{18}(6^1 3^2)$ 3 orthogonal experiment design plan, it was necessary to conduct another experiment for these levels.

In the verification experiment conducted for colemanite, 98.42% H_2O removal was calculated for 650 °C, 6 h, and 1 g ore amount. In the verification experiment conducted for ulexite, 99.1% H_2O removal from ulexite ore was calculated for 350 °C, 6 h, and 1 g ore amount. These values are the highest H_2O removal values reached as a result of dehydration experiments. This shows that the required value in the Taguchi method has been achieved.

Table 3. Experimental plan to be used in optimizing the dehydration of colemanite and ulexite ores and the obtained H_2O removal amounts.

Time (h)	Amount of ore (g)	Dehydration temperature (°C)		Total amount of H_2O remaining in the ore after the dehydration process (%)	
		Colemanite	Ulexite	Colemanite	Ulexite
2	1	400	50	9.44	34.66
4	3	400	50	8.38	34.81
6	5	400	50	7.30	34.51
2	1	450	100	3.64	30.27
4	3	450	100	4.85	24.79
6	5	450	100	5.48	29.09
2	3	500	150	4.15	29.50
4	5	500	150	4.09	23.52
6	1	500	150	3.64	22.21
2	5	550	200	2.17	9.15
4	1	550	200	2.92	8.51
6	3	550	200	2.80	7.50
2	3	600	250	3.40	5.82
4	5	600	250	1.88	4.62
6	1	600	250	1.95	4.67
2	5	650	300	1.72	3.09
4	1	650	300	0.70	2.63
6	3	650	300	1.33	1.39

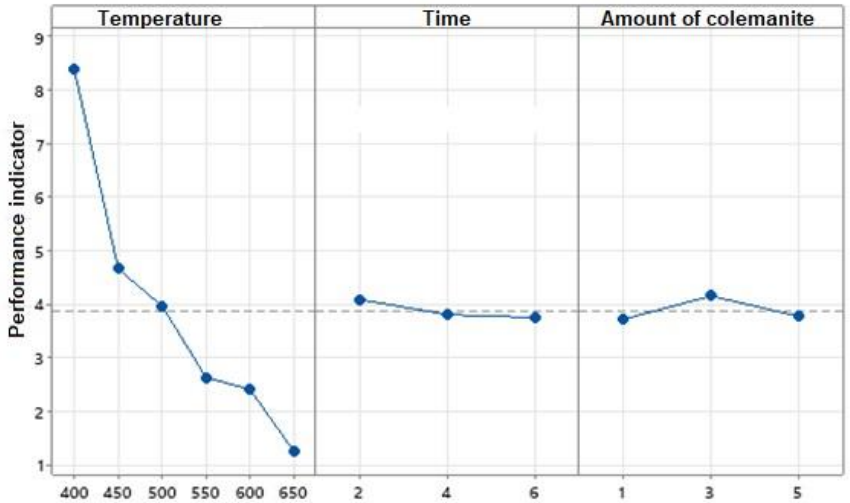

Fig. 3. According to the data obtained as a result of optimization experiments, the effect of temperature, time, and ore amount on the total H_2O amount (colemanite).

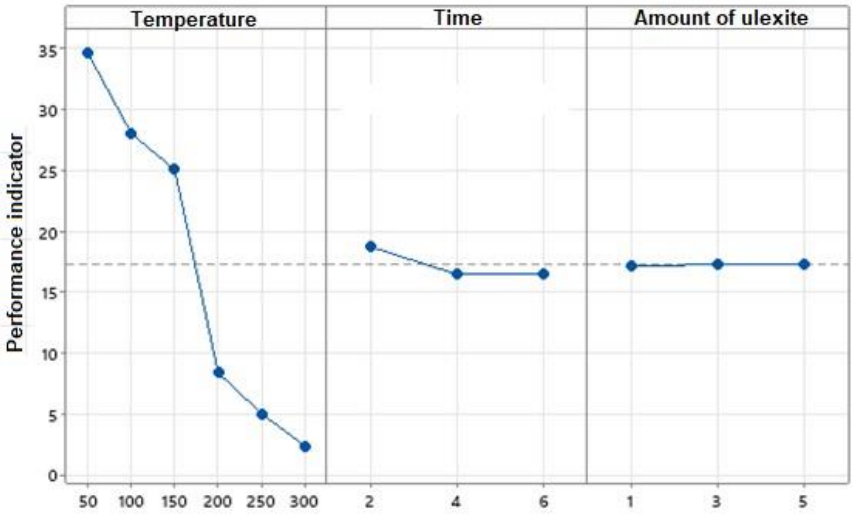

Fig. 4. According to the data obtained as a result of optimization experiments, the effect of temperature, time, and ore amount on the total H_2O amount (ulexite).

In the optimization study, the response table for the averages of colemanite and ulexite ores is given in Table 4, and the model summary is given in Table 5. The regression equation obtained for the total amount of H_2O removed was calculated with Eq. (2) (for colemanite) and Eq. (3) (for ulexite).

$$\text{Total amount of } H_2O \text{ removed} = (3.880+4.493\ \text{colemanite temperature\_400}+0.777\ \text{colemanite temperature\_450} + 0.08\ \text{colemanite temperature\_500} -1.25\ \text{colemanite temperature\_550}+1.47\ \text{colemanite temperature\_600} - 2.63\ \text{colemanite temperature\_650} - 0.165\ \text{amount of ore\_1} + 0.272\ \text{amount of ore\_3} - 0.107\ \text{amount of ore\_5}\ 0.207\ \text{duration\_2} - 0.077\ \text{duration\_4} - 0.130\ \text{duration\_6}) \quad (2)$$

$$\text{Total amount of } H_2O \text{ removed} = (17.263+ 17.40\ \text{ulexite temperature\_50}+ 10.79\ \text{ulexite temperature\_100}+ 7.81\ \text{ulexite temperature\_150} - 8.88\ \text{ulexite temperature\_200} - 12.23\ \text{ulexite temperature\_250} - 14.89\ \text{ulexite temperature\_300}+ 1.485\ \text{time\_2} - 0.783\ \text{time\_4} - 0.702\ \text{duration\_6} - 0.105\ \text{amount of ore\_1} + 0.038\ \text{amount of ore\_3} + 0.067\ \text{amount of ore\_5}) \quad (3)$$

Table 4. Response table for means.

Level	Colemanite			Ulexite		
	Dehydration temperature (°C)	Time (h)	Amount of ore (g)	Dehydration temperature (°C)	Time (h)	Amount of ore (g)
1	8.373	4.087	3.715	34.660	18.748	17.158
2	4.657	3.803	4.152	28.050	16.480	17.302
3	3.960	3.750	3.773	25.077	16.562	17.330
4	2.630	-	-	8.387	-	-
5	2.410	-	-	5.037	-	-
6	1.250	-	-	2.370	-	-
Delta	7.123	0.337	0.437	32.290	2.268	0.172
Rank	1	3	2	1	2	3

Table 5. Model summary.

	S	R-sq	R-sq(adj)	PRESS	R-sq(pred)	AICc	BIC
Colemanite	0.826	94.59%	88.51%	27.61	72.62%	95.59	61.38
Ulexite	1.96128	98.92%	97.70%	155.788	94.52%	126.73	92.53

Effects of the factors on H_2O removal are seen according to the variance analysis results from Table 6. While the dehydration temperature of colemanite ore was effective within the 94.32% confidence interval, the ulexite ore dehydration temperature was found within the 98.21% confidence interval. Duration and ore amounts are less effective for both ores.

Table 6. Analysis of variance for colemanite and ulexite ores.

Colemanite							
Parameters	DF	Seq SS	Distribution (%)	Adj SS	Adj MS	F-Value	P-Value
Temperature (°C)	5	94.320	93.53	94.3199	18.8640	27.67	0.000
Time (h)	2	0.674	0.67	0.6744	0.3372	0.49	0.627
Amount of ore (g)	2	0.393	0.39	0.3929	0.1965	0.29	0.757
Error	8	5.454	5.41	5.4538	0.6817	-	-
Total	17	100.841	100.00	-	-	-	-
Ulexite							
Parameters	DF	Seq SS	Distribution (%)	Adj SS	Adj MS	F-Value	P-Value
Temperature (°C)	5	2790.43	98.21	2790.43	558.085	145.08	0.000
Time (h)	2	19.87	0.70	19.87	9.934	2.58	0.136
Amount of ore (g)	2	0.10	0.00	0.10	0.051	0.01	0.987
Error	8	30.77	1.08	30.77	3.847	-	-
Total	7	2841.17	100.00	-	-	-	-

3.2. Dehydration experiments

In the dewatering experiments, colemanite and ulexite ores were weighed as 1, 3, 5 g, placed in porcelain crucibles, placed in the furnace and the experiments started. After the heat treatment at temperatures of 300-650 °C for colemanite and 50-350 °C for ulexite, weight differences were taken and the amount of water removed was determined. It was aimed to remove more than 90% of the water content of the ores at the beginning of the experiment. According to the chemical formulas of colemanite and ulexite minerals, it was determined that 1 g of B_2O_3 contains 0.2185 g and 0.354 g of crystal water, respectively. Calculations made after the dehydration experiments were completed showed that while the H_2O content decreased, the B_2O_3, Na_2O and CaO concentrations increased.

As a result of the experiments, 99.56% of the water in the colemanite ore was removed at 650 °C, 1 g of ore, and a period of 6 hours. As can be seen from Fig. 5, H_2O removal amounts were more efficient in the use of 1 g of ore. As a result of the experiments conducted with 1 g of ore, the lowest water removal amount was found to be 98.31% at the end of a 1-hour period at 650 °C (Fig. (5a)). In dehydration processes performed with 1 g ore samples, approximately 94% of the existing water could be removed even after 4 hours. Values close to these results were obtained for 3 and 5 g ore samples (Figs. 5(c-e)).

When looking at the changes in the H_2O amounts of ulexite ore Figs. 5(b-d-f), it is seen that the water contents begin to decrease in 1, 3, and 5 g ore samples in the temperature range of 50-100 °C. The increase in water loss was accelerated in the temperature range of 150-200 °C and reached its maximum level in the temperature range of 200-350 °C. Above 350-400 °C, the decrease in the amount of H_2O became stable, and almost all (99.5%) of the water in the ore was removed. It is seen that the weight decrease that occurs in dehydration processes after 50 °C corresponds to the physical release of water. As a result of the experiments, 99.67% of the water in the ore was removed at 350 °C, 1 g of ore and a period of 6 hours (Fig. 5(b)) (Şener and Özbayoğlu 2000).

As a result of the experiments, it is seen that there is an increase in B_2O_3 concentrations in both ores (Figs. 6(a-c-e)). For colemanite ore, the amount of B_2O_3, which was 50.97% at the beginning of the experiments, reached its maximum value of 64.93% at the end of 650 °C, 1 g ore, and 6 hours (Fig. 6(a)). As can be seen from Fig. 6, B_2O_3 amounts are higher when using 1 g of ore. As a result of the experiments, it is seen that there is an increase in the amount of B_2O_3 in ulexite ore, similar to that in colemanite ore (Figs. 6(b-d-f)). The amount of B_2O_3, which was 43.1% at the beginning of the dehydration experiments, reached its maximum value of 66.57% at the end of 350 °C, 1 g ore, and 6 hours (Şener and Özbayoğlu 2000; Kayandanet al. 2004; Eti Maden 2022).

As a result of the experiments, it was determined that there was an increase in the amount of CaO in both ores. The CaO amount of 27.18% determined for colemanite at the beginning of the experiments reached its maximum value of 34.63% at the end of 650 °C, 1 g of ore and 6 hours. As can be seen from the graph drawn according to the data obtained as a result of dehydration experiments, CaO amounts were more efficient in the use of 1 g of ore (Figs. 7(a-b-c)). Similar results were found for ulexite. The CaO amount of 13.8%, which was calculated at the beginning of the experiments for ulexite, reached its maximum value of 21.3% at the end of the experiments at 350 °C, 1 g of ore, and a period of 6 hours (Figs. 7(b-d-f)).

When the amount of Na_2O found in ulexite ore, unlike colemanite, was examined; there was also an increase in the amount of Na_2O. The amount of Na_2O, which was 7.6% at the beginning of the dehydration experiments, reached its maximum value of 11.79% at the end of 350 °C, 1 g ore, and 6 hours (Figs. 8(a-b-c)).

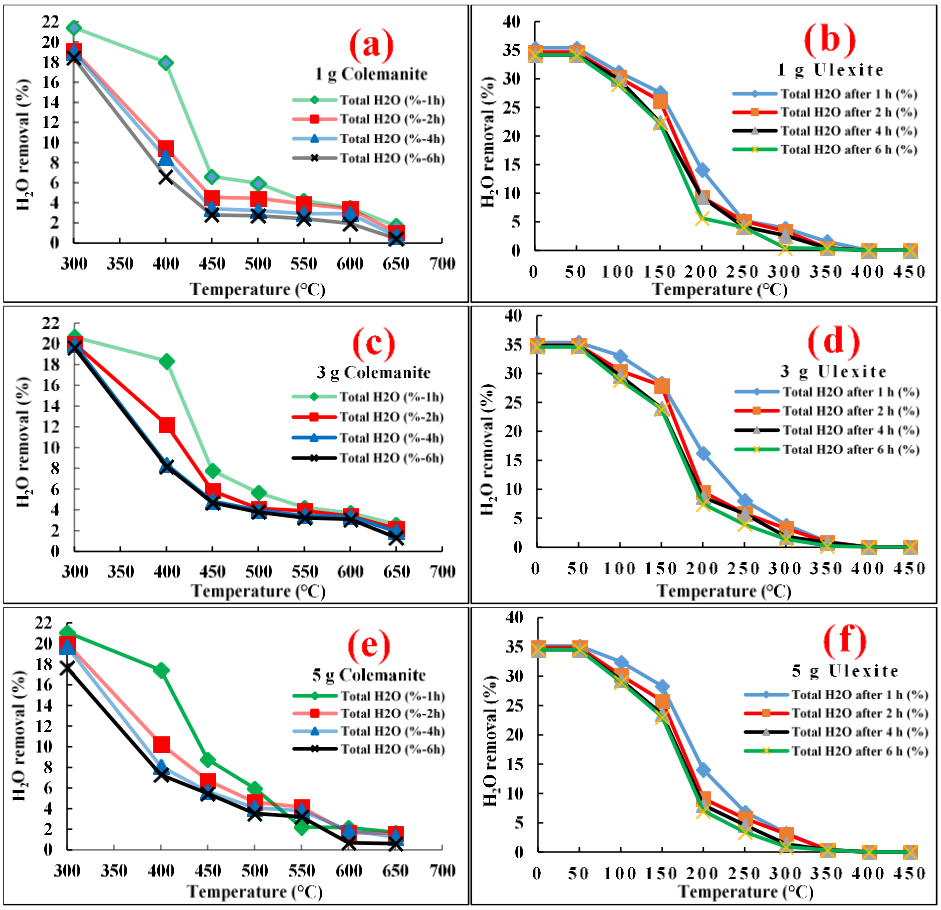

Fig. 5. H_2O removal amounts of 1, 3 and 5 g colemanite and ulexite ores after 1, 2, 4 and 6 hours of dehydration (%).

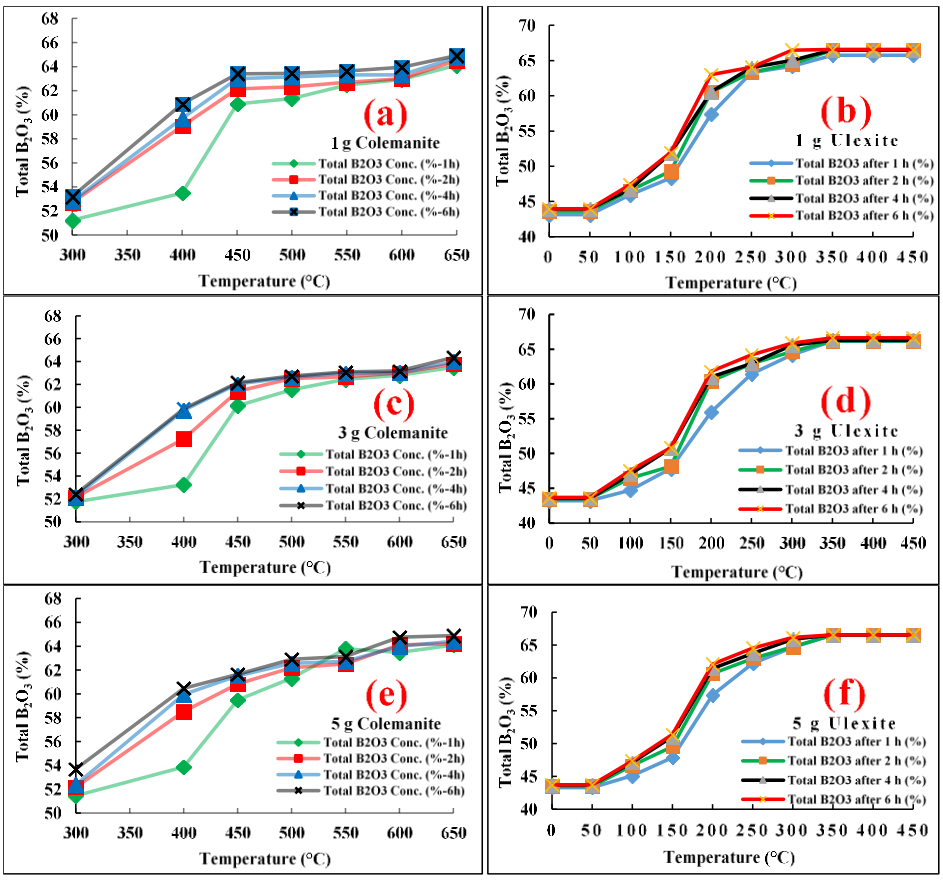

Fig. 6. B_2O_3 concentrations of 1, 3, and 5 g colemanite and ulexite ores after 1, 2, 4, and 6 hours of dehydration (%).

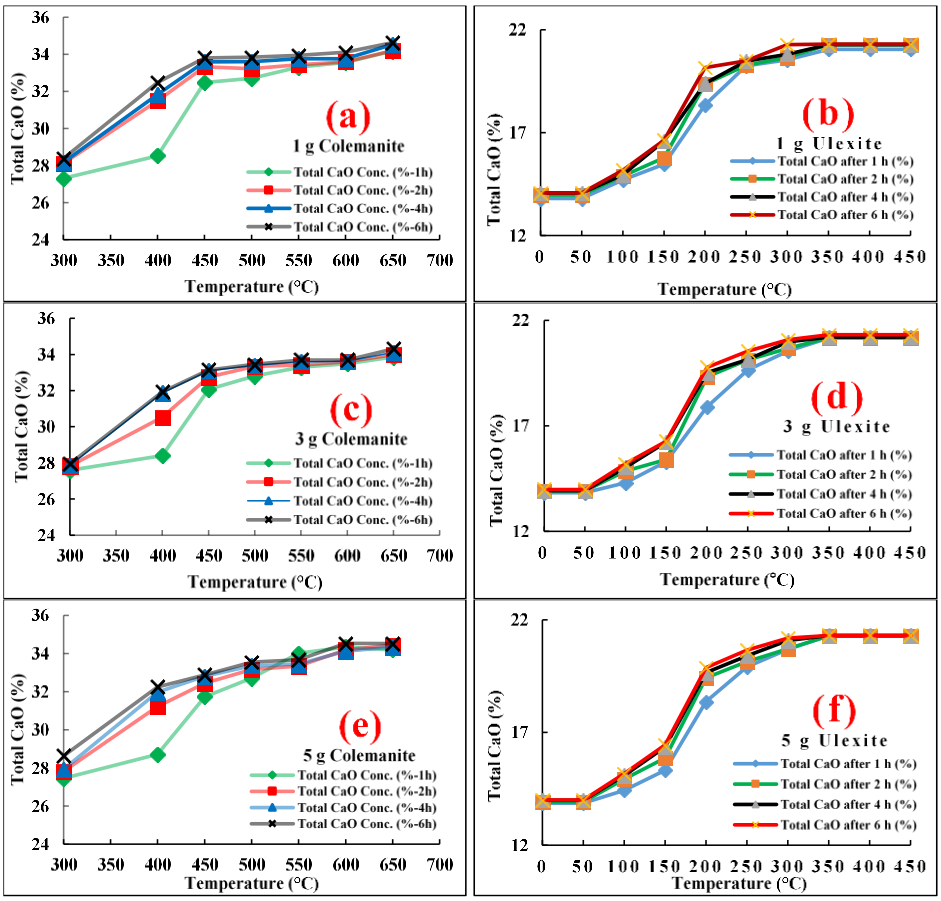

Fig. 7. CaO concentrations of 1, 3, and 5 g colemanite and ulexite ores after 1, 2, 4, and 6 hours of dehydration (%).

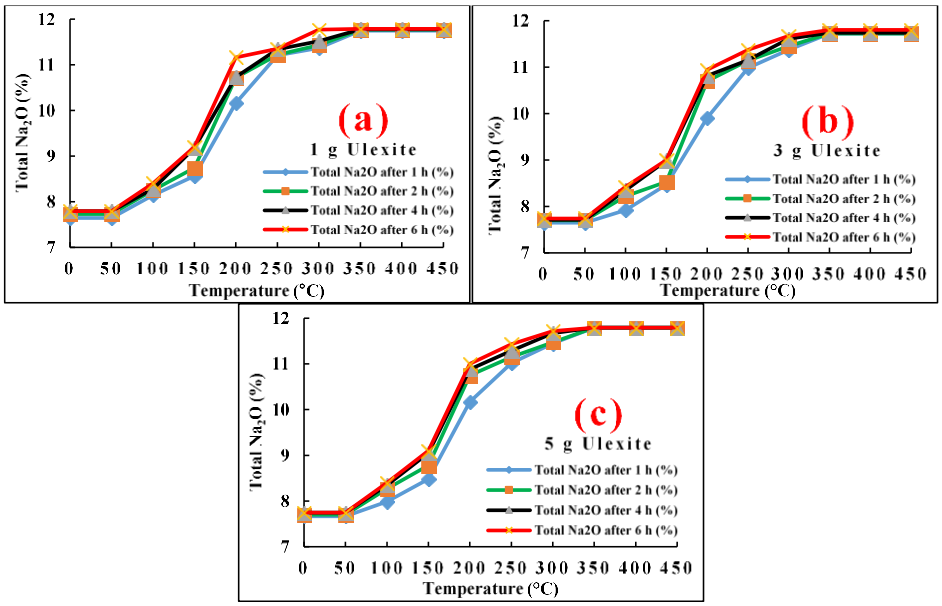

Fig. 8. Na_2O concentrations of 1, 3, and 5 g colemanite and ulexite ores after 1, 2, 4, and 6 hours of dehydration (%).

3.3. Optimization

The data obtained as a result of the experiments carried out according to the parameters selected for the optimization processes carried out by applying the Taguchi Method and the verification experiments carried out with the dehydration experiments are given comparatively in Table 7. When Table 7 is examined; Among the parameters selected according to the Taguchi Method, the parameters with the highest values are as follows: for colemanite ore; 650 °C, 4 h and 3 g ore amount, and for ulexite ore: 300 °C, 6 h and 3 g ore amount. In Tables 5 and 6, the effects of the factors on H_2O removal were examined according to the analysis of variance results. It

was determined that dehydration temperature was more effective, while time and ore amounts were less effective, in the confidence intervals of 98.21% (for colemanite) and 94.32% (for ulexite).

Table 7. Validation of the experimental results.

Ore	Temperature (°C)	Time (h)	Amount of ore (g)	Optimization-Verification			
				H_2O	B_2O_3	CaO	Na_2O
Colemanite	400	2	1	9.44	59.06	31.50	-
	400	4	3	8.38	59.75	31.87	-
	400	6	5	7.29	60.46	32.25	-
	450	2	1	4.53	62.15	33.32	-
	450	4	3	4.84	62.06	33.10	-
	450	6	5	5.47	61.65	32.88	-
	500	2	3	4.15	62.51	33.34	-
	500	4	5	4.08	62.56	33.36	-
	500	6	1	2.70	63.45	33.85	-
	550	2	5	4.15	62.51	33.34	-
	550	4	1	2.91	63.32	33.77	-
	550	6	3	3.22	63.09	33.69	-
	600	2	3	3.40	63.00	33.60	-
	600	4	5	1.88	63.99	34.13	-
	600	6	1	1.94	63.95	34.11	-
	650	2	5	1.60	64.20	34.44	-
	650	4	1	0.69	64.77	34.54	-
	650	6	3	1.32	64.36	34.32	-
	650	6	1	0.44	64.93	34.63	-
Ulexite	50	2	1	34.66	43.65	13.97	7.73
	50	4	3	34.81	43.54	13.93	7.71
	50	6	5	34.51	43.74	14.00	7.75
	100	2	1	30.27	46.58	14.90	8.25
	100	4	3	24.79	47.00	15.04	8.35
	100	6	5	29.09	47.39	15.17	8.40
	150	2	3	29.50	48.15	15.41	8.53
	150	4	5	23.52	51.05	16.35	9.05
	150	6	1	22.21	51.96	16.63	9.20
	200	2	5	9.15	60.68	19.42	10.75
	200	4	1	8.51	60.55	19.38	10.73
	200	6	3	7.50	61.79	19.77	10.94
	250	2	3	5.82	62.91	20.13	11.14
	250	4	5	4.62	63.71	20.39	11.29
	250	6	1	4.67	64.05	20.49	11.35
	300	2	5	3.09	64.73	20.71	11.47
	300	4	1	2.63	65.04	20.81	11.52
	300	6	3	1.39	65.86	21.08	11.67
	350	6	1	0.49	66.46	21.27	11.77

As a result, the parameter values that give the best results using the Taguchi method are; are for colemanite 650 °C for temperature, 6 h for time and 1 g ore amount, for ulexite 350 °C, 6 h for time and 1 g ore amount. Since the obtained levels were not included in the orthogonal experimental design plan, additional experiments were conducted for these levels, the obtained values are shown in Table 7 (with red color) and the results were confirmed.

3.4. Thermal analysis

Structural or chemical changes that may occur in colemanite ore were determined by TG/DTA analysis and compared with dehydration test results. The changes occurring here are explained by the temperatures at which the endothermic and exothermic peaks obtained during the measurement occur (Figs. 9 and 10). When the TG/DTG curves of the colemanite mineral were examined, no mass change occurred at temperatures up to 300 °C. It was observed that heating from 300 to 800 °C led to mass losses in two consecutive steps. It is seen that the colemanite sample undergoes rapid water loss in the temperature range of approximately 350 °C-450 °C, where an endothermic reaction occurs and thermal decomposition occurs. According to the DTA curve, it was determined that there were sharp peaks in the range of approximately 389°C-404 °C. Rapid water loss and irregular stresses in the crystal matrix cause expansion in the ore structure, allowing crystal transformation to occur as the temperature increases in the fractures that occur as a result of these internal stresses (Çelik and Suner 1995).

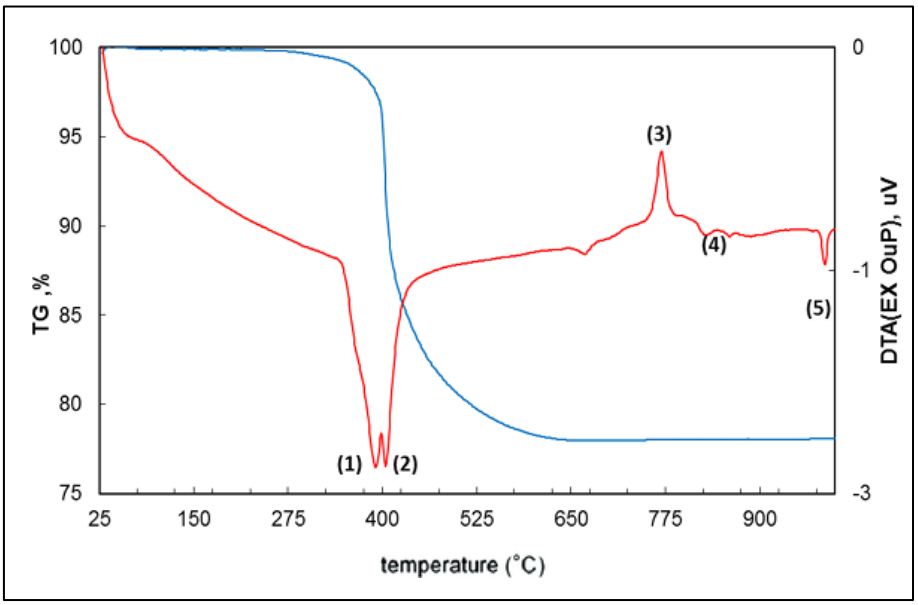

Fig. 9. TG/DTA curve of colemanite ore.

It has been determined that the decomposition of the ulexite mineral begins at 76°C and continues up to 240 °C. According to the TG/DTA curve, it was determined that there were 8% and 17% mass losses at the peaks at 146°C and 173°C. As heating continued, removal of the remaining OH– groups occurred, with peaks at 398°C and 718°C. It has been determined that water is completely released at temperatures up to 600 °C. As seen in Fig. 10, while a mass loss of approximately 14% occurred in the first stage, a mass loss of 4% was observed after 400 °C. The maximum peaks for these mass losses were determined from the TG/DTA curve as 109°C and 447°C, respectively.

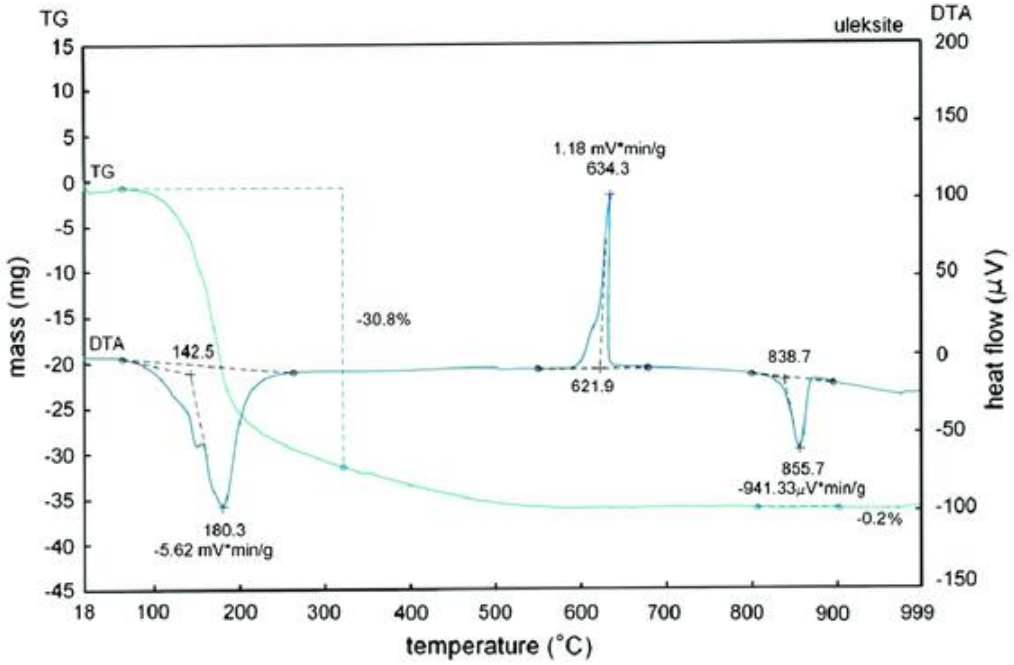

Fig. 10. TG/DTA curve of ulexite ore.

4. Conclusions

In this study, the dehydration of colemanite and ulexite ores and their optimization according to the Taguchi method were investigated in order to obtain anhydrous boron ores that can be used in cement production. The results found at the end of the study are stated as follows;

It was determined that approximately 98% of the chemically bound water in the colemanite ore was removed in the temperature range of 650-700 °C, the B_2O_3 grade increased to 65% and the amount of CaO increased to 35%. It was determined that approximately 99% of the chemically bound water in the ulexite ore was removed in the temperature range of 350-400 °C, the B_2O_3 grade increased to 67%, the amount of CaO increased to

21% and the amount of Na_2O increased to 12% (Yıldız 2004; Kayandan et al. 2004; Eti Maden 2022).

The optimum parameters determined according to the Taguchi method are (for colemanite) 650 °C temperature, 6 h time, and 1 g ore amount and (for ulexite) 350 °C, temperature, 6 h time, and 1 g ore amount (Kızılca and Çopur 2017). To determine the experimental plan selected according to the Taguchi Method, it has been proven that optimum results can be achieved with the orthogonal layout experimental design method $L_{18}(6^1 3^2)$ 3 factors, 18 experiments.

As a result of dehydration processes, it has been observed that colemanite and ulexite ores release the chemically bonded water they contain after a certain temperature and time by giving off heat to the environment and undergoing structural changes. The minerals, which were dehydrated by leaving their chemically bonded waters, crumbled to micronized sizes. Amorphous structures were observed at temperatures above 600-650 °C. While the decrease in the amount of crystal water depending on the ore amounts was around 1% at the initial temperatures, approximately 99% of the crystal water was removed at 350-450 °C in ulexite and at 600-700 °C in colemanite (Şener and Özbayoğlu 1994).

In dehydration experiments, solubility was decreased at temperatures above 450 °C (for ulexite) and 650 °C (for colemanite). It has been determined that run-of-mine ulexite and colemanite ores should be calcined in the temperature range of 350-350 °C and 650-700 °C, respectively. It has been shown that no treatment is required above these temperatures. It has been determined that as a result of the dehydration processes performed on run-of-mine ulexite ores for use in industrial applications, the tenors of colemanite and ulexite ores increase and anhydrous boron ore can be obtained (Kayandan et al. 2004; Eti Maden 2022).

The calcined colemanite ore crumbles into microns, but the main impurity, the clayey materials, leaves its amorphous structure and turns into a more shaped structure under the influence of the calcination temperature. When the sample containers are examined, it is seen that the sample surface is smooth. When mixed, it was observed that the parts that were slightly larger in terms of density and size were collected at the bottom. This reveals that during dehydration, the vapor of chemically bound water mixes the sample as it leaves the environment, and thus classification occurs. Such observations also reveal that the sample is calcined. It is seen that the weight reduction that occurs in dehydration processes corresponds to the physical release of water (Şener and Özbayoğlu 1994).

Using the Taguchi Method, the number of experiments to be carried out in the dehydration process was reduced to 18 experiments, and optimum results and parameters were achieved through this design. In this way, it has been shown that the necessary savings can be achieved in terms of economy and time, and the same results can be obtained with a small number of experiments (Altıner 2018). This means that additional dehydration/calcination costs can be avoided, production costs can be reduced, and transportation and energy costs can be saved. This situation is expected to bring many advantages, especially in terms of marketing (Oruç et al. 2004). Because it is known that chemically bound water and other impurities in boron minerals increase transportation and energy costs in boric acid production. For this reason, boric acid producers primarily prefer "anhydrous" boron ores. In this way, it has been shown that the cost of additional enrichment can be reduced, sales prices can be increased, thus making a significant contribution to the economy, and the desired quality of boron ores can be obtained in a very short time.

The accuracy of the experiments was supported by comparing the data obtained as a result of both optimization and dehydration experiments with thermal analyses. The next step of this study should be studies on the use of boron ores in cement production according to their water content ratios.

Acknowledgements

None declared.

Funding

The authors received no financial support for the research, authorship, and/or publication of this manuscript.

Conflict of Interest

The authors declared no potential conflicts of interest with respect to the research, authorship, and/or publication of this manuscript.

Author Contributions

All of the authors made substantial contributions to conception and design, or acquisition of data, or analysis and interpretation of data; were involved in drafting the manuscript or revising it critically for important intellectual content; and gave final approval of the version to be published.

Data Availability

The datasets created and/or analyzed during the current study are not publicly available, but are available from the corresponding author upon reasonable request.

REFERENCES

Akyıldız A (2012). Beton Üretiminde Bor Atıklarının Puzzolan Materyal Olarak Kullanılabilirliğinin Araştırılması. *Ph.D. thesis*, Namık Kemal University, Tekirdağ, Türkiye,

Altıner M (2018). Study of using calcium carbide slag to prepare calcium oxide briquettes by molding and calcination processes through Taguchi method*. Cukurova University Journal of the Faculty of Engineering*, 33(1), 179–188.

Baynal K (2005). Çok yanıtlı kalite karakteristiklerinin eş zamanlı eniyilenmesinde Taguchi yöntem ve otomotiv endüstrisinde bir uygulama. *Journal of Industrial Engineering*, 16(2), 2-8. (in Turkish)

Boren (2016). Yapı Malzemelerinde Bor, Bor ve Kullanım Alanları*, National Boron Research Institute*. http://www.boren.gov.tr/tr [accessed 10-10-2023].

Celik MS, Suner F (1995). A thermodynamic analysis of the decrepitation process. *Thermochimica Acta,* 245, 167-174.

Çelik H (2007). Üleksit Cevherinin Perklorik Asit Çözeltilerindeki Çözünürleştirme Kinetiği, Kalsinasyonu ve Optimizasyonu. *M.Sc. thesis*, Yüzüncüyıl University, Van, Türkiye.

Çelik MS, Uzunoğlu HA, Arslan, F (1994). Decrepitation properties of some boron minerals. *Powder Technology*, 79, 167-172.

Çopur M, Özmetin C, Özmetin E, Kocakerim MM (2004). Optimization study of the leaching of roasted zinc sulphide concentrate with sulphuric acid solutions. *Chemical Engineering and Processing*, 43, 1007-1014.

Danışman E, Yalçındağ Y (2023). Process improvement and an application with Taguchi method in food industry. *Journal of Yaşar University*, 16(69), 105-131.

Demirel B, Nasıroğlu S (2017). Bor mineralleri ve atıklarının çimentoda kullanılma stratejileri. *Science and Engineering Journal of Fırat University*, 29(1), 95-100. (in Turkish)

DPT (2001). Madencilik Özel İhtisas Komisyonu Raporu. Endüstriyel hammaddeler Alt Komisyonu, Kimyasal Sanayi Hammaddeleri. Cilt-II. Sekizinci Beş Yıllık Kalkınma Planı, Devlet Planlama Teşkilatı, Ankara, Türkiye. https://www.sbb.gov.tr/wp-content/uploads/2022/08/Sekizinci-Bes-Yillik-Kalkinma-Plani-Madencilik-OIK-Raporu EndustriyelHammaddelerAltKomisyonu-GenelEndustriMineralleri-Calisma-GrubuRaporu.pdf [accessed 10-10-2023].

Durmuş C (2016). Bor Katkılı Çimentoların Özelliklerinin İncelenmesi. *M.Sc. thesis*, Dokuz Eylül University, İzmir, Türkiye. (in Turkish)

Elbeyli İY, Derun EM, Gülen J, Pişkin S (2003). Thermal analysis of borogypsum and its effects on the physical properties of Portland cement. *Cement and Concrete Research*, 33, 1729-1735.

Eti Maden (2022). Bor Sektör Raporu, Strateji Geliştirme Dairesi Başkanlığı, Eti Maden İşletmeleri Genel Müdürlüğü. https://www.etimaden.gov.tr/storage/pages/June2022/2021%20YILI%20BOR%20SEKTÖR%20RAPORU.pdf [accessed 10-10-2023].

Eyyüboğlu S (2013), Kolemanit Konsantratör Atıklarının Çimento Üretiminde Değerlendirilmesi. *M.Sc. thesis*, Balıkesir University, Balıkesir, Türkiye. (in Turkish)

Helvacı C (2015). Bor yataklarının mineral ve kimyası yönünden genel değerlendirilmesi ve gelecek öngörüsü. *Madencilik ve Yer Bilimleri Dergisi*, 6(47), 66-78. (in Turkish)

Helvacı C (2017). Borate deposits: An overview and future forecast with regard to mineral deposits, *Journal of Boron*, 2(2), 59-70.

Kayandan İ, Pehlevan V, Çağlayan,B, Türedi S (2004). Düşük tenörlü kolemanit cevherinin kalsinasyon yöntemi ile zenginleştirilmesi. *International Boron Symposium*, Eskişehir, Türkiye, 65-69. (in Turkish)

Kılcı S (2011). Borik Asitin Dehidratasyonu. *M.Sc. thesis*, Sakarya University, Sakarya, Türkiye. (in Turkish)

Kızılca M, Çopur M (2017). An optimization study on dissolution of the calcined colemanite mineral in methyl alcohol by CO2 in an autoclave system using Taguchi method. *2nd World Conference on Technology, Innovation and Entrepreneurship,* Istanbul, Türkiye, PAP-WCTIE-V.5-2017(28), 198-204.

Kocadağistan ME (2007), Çayeli Yöresi Bakır Cevherlerinin Biyoliçi. *Ph.D. thesis*, Atatürk University, Erzurum, Türkiye. (in Turkish)

Kumsal KH (1994). Taguchi Metodu. *M.Sc. thesis*, İstanbul University, İstanbul, Türkiye. (in Turkish)

Kurtuluş C, Kurtuluş R (2021). Surface modification of anhydrous borax with stearic acid by wet coating method. *Journal of Characterization*, 1(1), 1-9.

Mercan Ş (2019). Improvement of Product Quality by Using Design of Experiment and Artificial Intelligence Techniques. *M.Sc. thesis*, Balıkesir University, Balıkesir, Türkiye.

Olgun A, Kavas T, Erdoğan Y, Önce G (2006). Physico-chemical characterictics of chemically activated cement containing boron. *Building and Environment*, 42, 2389-2395.

Oruç F, Sabah E, Erkan ZE (2004). Türkiye'de bor atıklarının sektörel bazda değerlendirme stratejileri. *II. International Boron Symposium*, Eskişehir, Türkiye, 385-392. (in Turkish)

Özden E (2020). Elektrostatic Powder Coating Process Parameteres' Optimization with Experimental Design Methods and Their Industrial Applications. *M.Sc. thesis*, Balıkesir University, Balıkesir, Türkiye.

Pehlivanoğlu HE, Davraz M, Kılınçarslan Ş (2013). Bor bileşiklerinin çimento priz süresine etkisi ve denetlenebilirliği. *SDU International Technologic Science*, 5(3), 39-48.

Samtaş G, Gülesin M (2005). Tolerans analiz yöntemleri ve Mak-tol tolerans analiz sistemi. *Journal of the Faculty of Engineering and Architecture of Gazi University,* 20(1), 85-93. (in Turkish)

Şanyılmaz M (2006). Deney Tasarımı ve Kalite Geliştirme Faaliyetlerinde Taguchi Yöntemi ile bir Uygulama. *M.Sc. thesis*, Dumlupınar University, Kütahya, Türkiye. (in Turkish)

Şener S, Özbayoğlu G (1994). Üleksitin kalsinasyon özelliklerinin tespiti ve üleksit kolemanit ayrılmasında kalsinasyonun kullanımı. *Bor Mineralleri Zenginleştirme Semineri Bildirileri*, Bornova, İzmir, Türkiye, 47-57. (in Turkish)

Şener S, Özbayoğlu G, Demirci Ş (2000). Changes in the structure of ulexite on heating. *Thermochimica Acta*, 362, 107-112.

Taguchi G, Chowdhury S, Taguchi S (1999). Robust Engineering. McGraw-Hill Publishing Company, TS156.T335, New York, USA.

Topçu U, Soyhan HS (2022). Bor minerallerinin yangın geciktirici etkileri, *Fuels, Fire and Combustion in Engineering Journal*, 10(1), 28-37. (in Turkish)

Tunç M, Erşahan H, Yapıcı S, Çolak S (1997). Dehydration kinetics of ulexite from thermogravimetric data. *Journal of Thermal Analysis and Calorimetry*, 48, 403-411.

Tunç M, Yapıcı S, Kocakerim MM, Yartaşi A (2001). The dissolution kinetics of ulexite in sulphuric acid solutions. *Chemical and Biochemical Engineering Quarterly*, 15(4), 175-180.

Ulusoy H (2012). Eskişehir Kırka Yöresinde Bor Madeni Çevresinde Yaşayan İlköğretim Çağındaki Çocuklarda Kan Bor Düzeyinin Ölçülmesi. *Medical dissertation*, Osmangazi University, Eskişehir, Türkiye. (in Turkish)

Yenialaca Ç (2009). Bor ve Kullanım Alanları. *M.Sc. thesis*, Gazi University, Ankara, Türkiye. (in Turkish)

Yıldız Ö (2004). The effect of heat treatment on colemanite processing: A Ceramics Application. *Powder Technology*, 142, 7-12.

Yılmaz M, Keskin M (2019). Determination of optimal reading conditions by Taguchi method. *Academic Platform Journal of Engineering and Science*, 7-1, 25-32.

Challenge Journal of Concrete Research Letters

Research Article

The effect of the gravity on the earthquake performance of roller compacted concrete dams

Fethi Şermet [a,*], Murat Emre Kartal [b], Muhammet Ensar Yiğit [c], Emin Hökelekli [d]

[a] *Department of Civil Engineering, Iğdır University, 76000 Iğdır, Türkiye*
[b] *Department of Civil Engineering, İzmir Demokrasi University, 35100 İzmir, Türkiye*
[c] *Department of Civil Engineering, Manisa Celal Bayar University, 45100 Manisa, Türkiye*
[d] *Department of Civil Engineering, Bartın University, 74000 Bartın, Türkiye*

ABSTRACT

Roller compacted concrete (RCC) is a dry concrete mixture often utilized in the construction of large dams. The interlayer of the RCC dam, which is the weakest plane of the structure, can easily fail under hydraulic shear load, geological impact, earthquake force and environmental impact. In this study linear and performance analyzes were carried out for eight different scenarios for foundation effect, gravity effect and empty and full reservoir situations. In analyses, the earthquake response and performance of the Akçakoca RCC Dam, taking into account the interaction between the dam and the water. The reservoir water behavior is simulated using the Eulerian-Lagrangian coupled (CEL) approach with finite elements modeling. Linear analyses reveal that hydrodynamic pressure leads to increased displacements and principal stresses. The earthquake performance evaluation of the Akçakoca RCC dam indicates that critical concrete damages are expected based on linear time-history analyses conducted for both empty and full reservoir scenarios. Besides, according to this study, gravity effect clearly increases the earthquake performance of the dam.

ARTICLE INFO

Article history:
Received 23 November 2023
Revised 10 January 2024
Accepted 3 February 2024

Keywords:
RCC dams
Gravity effect
Hydromechanics
Structure dynamics
Performance analysis

1. Introduction

In recent years, the roller compacted concrete (RCC) dam has become increasingly popular as a modern dam construction method. RCC dams possess comparable structural strength to traditional concrete dams, and their construction process, resembling the technique used for roller compaction soil-rock dams, enhances operational efficiency in the field.

The increasing need for renewable energy has led to the construction of numerous high concrete dams, especially in seismically active regions. For example, there are many dams higher than 150 m in Türkiye. These dams are designed to withstand high foundation acceleration values, such as 0.50 g. Ensuring the seismic safety of these concrete dams is of paramount importance in the field of engineering. The seismic events possess the capability to interfere with the effective operation of these essential infrastructures, causing disastrous breakdowns that may lead to substantial human and property losses. Consequently, ensuring the seismic resilience of these dams has emerged as a vital focus for engineers and researchers.

Various theoretical methods have been suggested to forecast dam deformations and assess the current operational condition of dams (He et al. 2018; Dou et al. 2019; Yang et al. 2019; Zhang et al. 2019). However, in real-world situations, the integration of roller compacted concrete (RCC) with conventional concrete (CC) becomes inevitable. In projects characterized by challenging geological conditions and demanding construction timelines, a blend of both roller compacted concrete (RCC) and conventional concrete (CC) may be employed in the design and construction phases of dams. RCC con-

* *Corresponding author*. Tel.: +90-476-223-0040 ; E-mail address: fethi.sermet@igdir.edu.tr (F. Şermet)
ISSN: 2548-0928 / DOI: https://doi.org/10.20528/cjcrl.2024.01.003

sists of the same components as conventional concrete: well-graded aggregates, cementitious materials, and water (Calis and Yıldızel 2019). The utilization of RCC in dam construction enables elevated productivity levels (Cervera et al. 2000), this approach can help in reducing construction time, compensating for delays in foundation treatment. It effectively relieves the pressure on the construction schedule, particularly for specific dam shapes. However, the distinct material properties and deformation characteristics of conventional concrete and roller compacted concrete raise concerns about structural safety. Specifically, notable deformation gradients are frequently observed at the interfaces where there are substantial volumes of diverse concrete materials (Luo et al. 2016).

The initiation, propagation, and coalescence of cracks within concrete structures are pivotal factors contributing to seismic damage and failure (Luo et al. 2016). Earthquake analyses on 2D finite fluid models in both linear and nonlinear time domains were conducted by Kartal et al. (2017), suggesting that the seismic behavior of the dam is impacted by the reservoir's length. Alembagheri (2020) introduced an approach to evaluate damage extent using linear seismic analysis results, with a specific focus on potential damage due to tension cracking in concrete. The methodology was illustrated and potential nonlinear responses and damage mechanisms were explored through the presentation of three examples involving concrete gravity dams. Wang et al. (2015) employed a two-dimensional fluid finite element approach incorporating the Lagrangian method for simulating the reservoir water. Considering the influence of dam reservoir-foundation interaction, they conducted a numerical investigation to predict potential failure modes of concrete gravity dams. Hariri-Ardebili et al. (2016) performed parametric finite element analyses on a standard concrete gravity dam. They modelled the unified dam-foundation-reservoir system using a Lagrangian-Eulerian approach. Their results suggested that primary potential failure modes of gravity dams include cracking along the length, cracking at the base, sliding, and overturning. Contrastingly, Huang (2018) introduced a comprehensive numerical framework for the analysis of seismic ruptures, which incorporates interactions among dam, reservoir, sediment, and foundation. This framework integrates a nonlinear extended finite element formulation, addressing material, geometric, and contact nonlinearities. Furthermore, it incorporates an adaptive time-stepping extended multiple transmission boundary. Applying this methodology, Sharma et al. (2020) explored the seismic cracking behavior of a representative concrete gravity dam system. They introduced a space-time finite element method for the dynamic rupture analysis of a dam-reservoir system supported on a completely rigid foundation. Similarly, Bayraktar et al. (2009) conducted earthquake performance analysis on the Torul Concrete Lined Rock Fill (CFR) Dam, utilizing two-dimensional finite element models and considering both dam-soil and dam-soil-reservoir interactions. In the analysis, a Lagrangian approach was utilized for fluid elements, and interface elements were incorporated to mimic the sliding behavior between the concrete surface slab and the rock fill material. These elements played a crucial role in accurately capturing the interactions and responses within the dam structure under seismic conditions. Liu et al. (2023) examined the risks of dam cracking during the construction phase, taking into account the spatial variability of thermodynamic parameters. Li et al. (2021) investigated the heightened risk of cracking in the dam body due to seismic damage in gravity dams, considering the spatial variability of tensile strength. This factor should be considered in seismic design. Additionally, there has been significant attention on time-varying reliability, as evidenced by previous studies (Wang et al. 2023; Liu et al. 2022; Li et al. 2022; Yin et al. 2023).

In this study, the impact of both gravity and earthquake forces on dam performance was investigated. The analysis encompassed eight different conditions, accounting for the dam body with and without foundation, considering gravity, and examining both full and empty dam conditions. Through these analyses, the performed solutions successfully determined the influence of foundation and gravity on the dam's performance.

2. Formulation of Eularian-Lagrangian Coupled Approach for Dam-Reservoir-Foundation Interaction

The Eulerian-Lagrangian Combined Approach is a useful method for investigating complex interactions within structures by considering both a broader spatial context and the behavior of individual elements. This comprehensive analysis aids in making informed decisions related to the safety, integrity, and risk assessment of structures. In the context of fluid dynamics and continuum mechanics, the Eulerian and Lagrangian definitions are two fundamental approaches used to analyze the movement and behavior of materials (Skrzat 2012).

The Eulerian-Lagrangian Coupled Approach is a robust method for studying complex interactions within dams, considering both overall spatial context and individual element behavior. This approach enables detailed analysis, aiding decisions on dam safety, structural integrity, and risk assessment. In fluid dynamics and continuum mechanics, Eulerian and Lagrangian descriptions are fundamental. Eulerian focuses on fixed spatial points, tracking property changes (e.g., velocity, pressure) over time. Lagrangian tracks individual particle motion, formulating equations based on specific particle properties, like position and velocity, at any given time.

The correlation between material and spatial time derivatives can be formulated as follows:

$$\frac{D\Phi}{Dt} = \frac{\partial \Phi}{\partial t} + v.(\nabla.\Phi) \quad (1)$$

In the context provided:

- In this expression, Φ denotes the arbitrary solution variable.
- The symbol v represents the material velocity.
- $D\Phi/Dt$ corresponds to the material time derivative.
- $\partial\Phi/\partial t$ signifies the spatial time derivative.

The equations conserving mass, momentum, and energy, initially developed within the Lagrangian framework, are transformed into Eulerian conservation equations that involve spatial derivatives. The specific process and methodology for this conversion are detailed in the reference provided by Benson and Okazawa (2004).

$$\frac{\partial \rho}{\partial t} + v.(\nabla.\rho) + \rho \nabla.v = 0 \quad (2)$$

$$\frac{\partial v}{\partial t} + v.(\nabla.v) = \frac{1}{\rho}(\nabla.\sigma) + b \quad (3)$$

$$\frac{\partial e}{\partial t} + v.(\nabla e) = \sigma : D \quad (4)$$

where ρ represents density, σ denotes the Cauchy stress, b is the vector of body forces, e stands for strain energy, and D represents velocity strain.

The equations in the Eulerian framework Eqs. (2) and (4) can be restructured into conservative formats as described in reference by Benson (1997).

$$\frac{\partial \rho}{\partial t} + \nabla.(\rho v) = 0 \quad (5)$$

$$\frac{\partial \rho v}{\partial t} + \nabla.(\rho v \otimes v) = \nabla.\sigma + \rho b \quad (6)$$

$$\frac{\partial e}{\partial t} + \nabla.(ev) = \sigma : D \quad (7)$$

$$\frac{\partial \phi}{\partial t} = S \quad (8)$$

$$\frac{\partial \phi}{\partial t} + \nabla.\varphi = 0 \quad (9)$$

The Eulerian governing Eqs. (5) and (7) have a general form:

$$\frac{\partial \phi}{\partial t} + \nabla.\varphi = S \quad (10)$$

where ϕ represents the flux function, and S represents the source term. Eq. (10) is divided into two equations and solved sequentially using operator splitting, as described in reference.

Eq. (8) encompasses the source term that signifies the Lagrangian step, whereas Eq. (9) incorporates the convective term, representing the Eulerian step.

The deformed mesh, derived from the Lagrangian step, is mapped onto the stationary Eulerian mesh to solve Eq. (9). Subsequently, the volume of material displaced between neighboring elements is calculated. Parameters of the Lagrangian solution, such as mass, stress, and energy, undergo adjustments throughout the process to accommodate the movement of material between adjacent regions. The Lagrangian step utilizes the virtual work principle, as elucidated in reference to Bathe (1996), to facilitate these modifications.

$$\int_v \rho a.\delta u dv + \int_v \sigma : \delta \varepsilon dV = \int_S t.\delta u dS + \int_v \rho b.\delta u dV \quad (11)$$

The updated Lagrangian formulation is appropriate for the Lagrangian step because it corresponds to the present configuration in the Eulerian approach, which aligns with the reference configuration at time t. Predicting the body's configuration at $t+\Delta t$, as specified in Eq. (11), is fundamentally difficult. This prediction incorporates unknown elements such as integration volume and density, both of which are affected by the body's deformations.

3. Case Study: Akçakoca RCC Dam

3.1. Akçakoca Dam

The Akcakoca Dam, located approximately 17 km north of Düzce, was constructed in 2016 by the State Hydraulic Works of Turkey (Fig. 1). It was specifically designed and built as a roller-compacted concrete dam near the Akçakoca mouth. The resulting reservoir, formed by the dam, primarily serves irrigation purposes. The dam crest has a length of 150 meters and a width of 8 meters. It reaches a maximum height of 66 meters, with a base width of 62 meters. The water level in the reservoir reaches its peak at 62 meters.

Fig. 1. Akçakoca Dam (DSİ 2023).

The effect of gravity is often neglected when determining earthquake performance. Therefore, it is important to determine to what extent gravity will affect the dam performance whether it is included in the calculations or not. In the context of this study, various models were developed, including gravity and non-gravity models, as well as models with and without a foundation rock. These models were further categorized into empty and full dam configurations, resulting in a total of 8 distinct models for the analysis, as outlined in Table 1.

Table 1. Dam analysis models.

Cases	Water conditions	Gravity	Model
Case 1	Empty	Without	Dam Body
Case 2	Full		
Case 3	Empty	With	
Case 4	Full		
Case 5	Empty	Without	Dam-Foundation
Case 6	Full		
Case 7	Empty	With	
Case 8	Full		

3.2. Material properties of Akçakoca Dam

Akçakoca Dam's two-dimensional finite element model has a single-layered gneiss rock foundation. Table 2 shows the material parameters of the Akçakoca roller compacted concrete dam body and its foundation. As a concrete property, a mixture containing 60 kg/m^3 cement, 30 kg/m^3 fly ash and 125 lt/m^3 water was used as RCC mixture.

3.3. Finite element modeling of Akçakoca Dam

In this research, a 2D finite element model (FEM) is developed for the critical section of the Akçakoca Roller Compacted Concrete (RCC) dam using ABAQUS software. The model defines the dam's height as 'H,' and the foundation rock extends 'H' units in both the downstream river and gravity directions. Additionally, the foundation rock and reservoir water model extend '3H' units upstream. The fluid and solid element matrices are computed using the Gauss numerical integration technique, as per the methodology outlined by Wilson and Khalvati (1983). Specifically, the dam body (C3D8) is subdivided into elements with 2×2 integration points, the foundation rock (C3D8) is also divided into elements with 2×2 integration points, and the fluid element (EC3D8) incorporates 2×2 integration points.

Table 2. Material properties of Akçakoca roller compacted concrete dam (Sunbul et al. 2018; Kartal and Karabulut 2018).

	Modulus of elasticity (GPa)	Poisson's ratio	Mass density (kg/m^3)
Concrete (Dam Body)	28	0.2	2500
Gneiss	18	0.15	2800
Water	2.2	-	1000

We analyzed the maximum tensile and compressive stresses with respect to the dam height. Following that, we illustrated the maximum principal tensile and compressive stresses experienced during an earthquake on the upstream side of the dam body. This study involved an investigation of four different scenarios to identify the most critical conditions of the dam, as detailed below (Figs. 2-5).

First condition involves empty reservoir and galleries are excluded from dam body. This model has totally 1540 nodal points and 714 elements. Second condition involves full reservoir dam body. Contact elements were defined for the interaction surface. This model has totally 8990 nodal points and 4270 elements. Third condition involves empty reservoir and galleries are excluded from dam body. This model has totally 6092 nodal points and 2844 elements. Fourth condition involves full reservoir and galleries are excluded from dam body. Contact elements were defined for the interaction surface. This model has totally 13542 nodal points and 6427 elements.

3.4. 1999 Düzce Earthquake

The Düzce Earthquake occurred on 12 November 1999 at 18.57 local time (16.57 UTC) with a moment magnitude of 7.2. This seismic event resulted in significant damage, causing 845 fatalities and 4948 injuries in Düzce, Türkiye. The epicenter was located at coordinates 40.768° latitude and 31.148° longitude, with a moment magnitude of 6.2 (Mb), surface wave magnitude of 7.4 (Ms), seismic moment (Mo) of 4.5×10^{19} Nm, and moment magnitude of 7.1 (Mw) (Erdik 2000). For this study, the North-South (N-S) and vertical components of the 1999 Düzce accelerogram were utilized, as depicted in Figs. 6-7.

Fig. 2. Creating a finite element model for a dam in the absence of water in the reservoir.

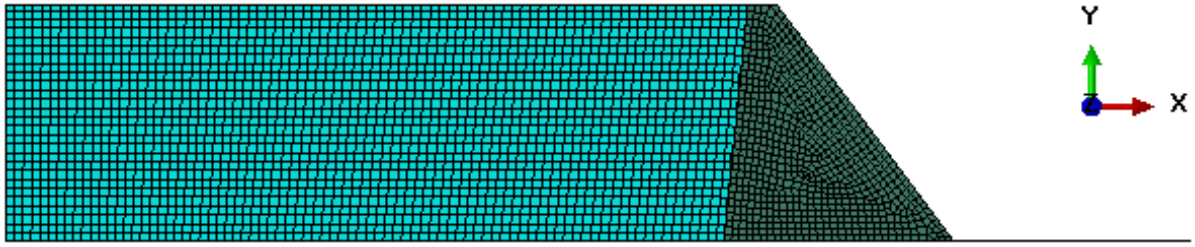

Fig. 3. Creating a finite element model for a dam with a full reservoir.

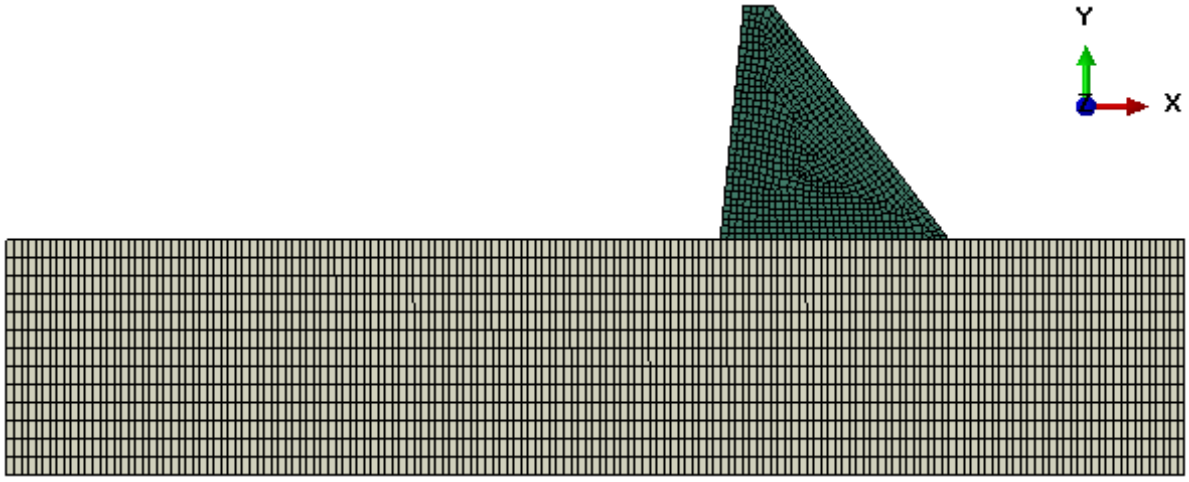

Fig. 4. Finite element model incorporating foundation rock for an empty reservoir.

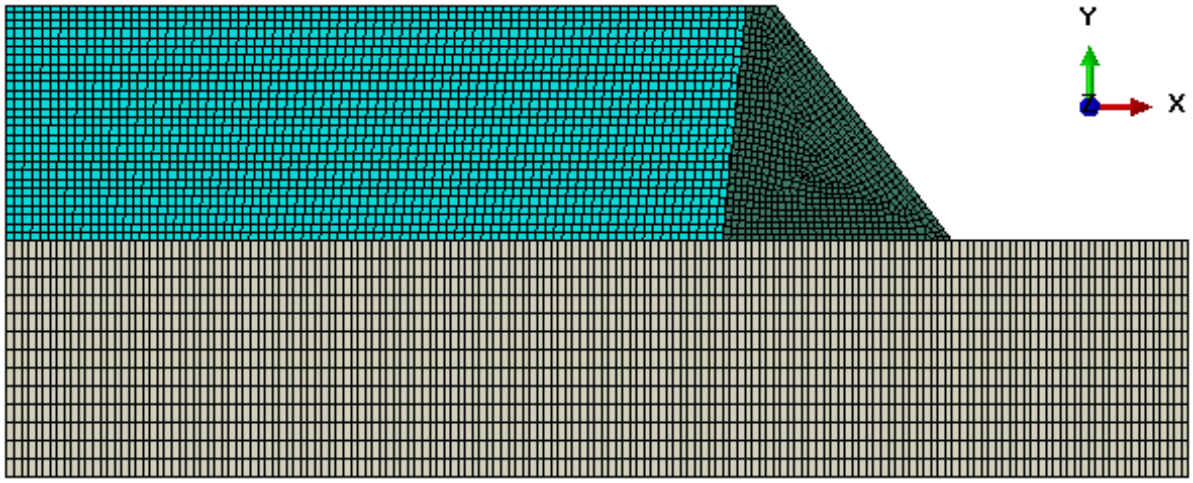

Fig. 5. Finite element model with foundation rock for a full reservoir.

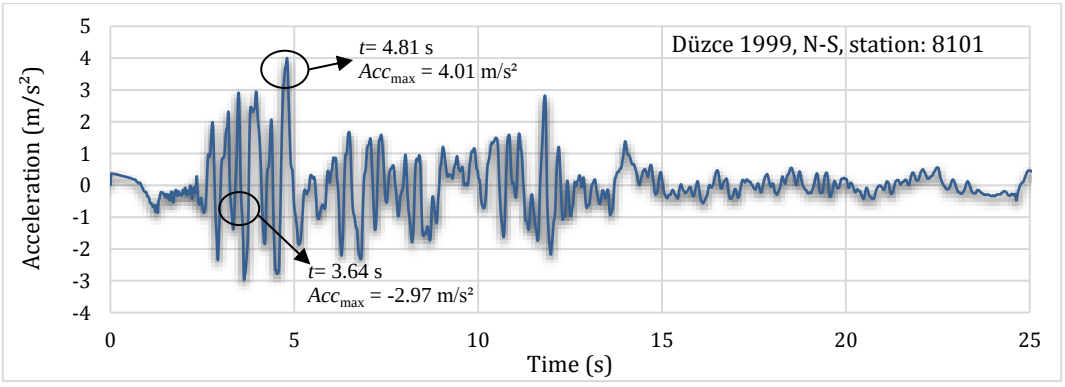

Fig. 6. 1999 Düzce Earthquake accelerogram for North-South direction (AFAD 2023).

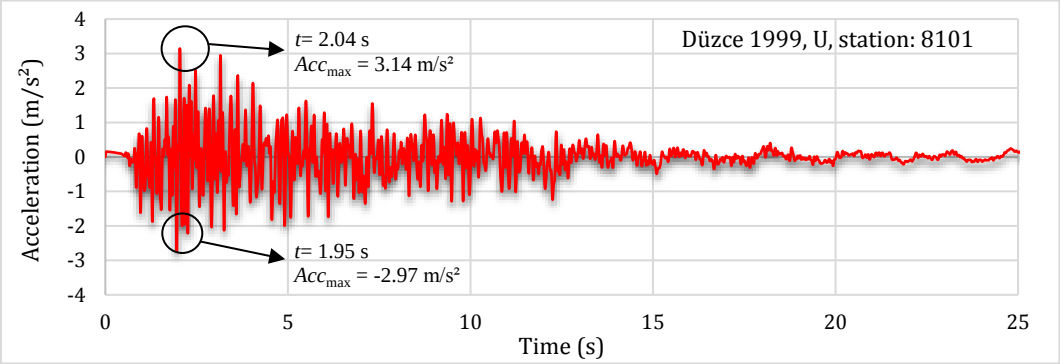

Fig. 7. 1999 Düzce Earthquake for vertical direction (AFAD 2023).

3.5. Optimum mesh density

In the upcoming numerical studies, it is crucial to create a finite element mesh that produces accurate results. To determine the optimal mesh, it is necessary to analyze various models with different numbers of finite element divisions and compare their outcomes. The finite element mesh plays a significant role, especially in areas where stress values suddenly increase.

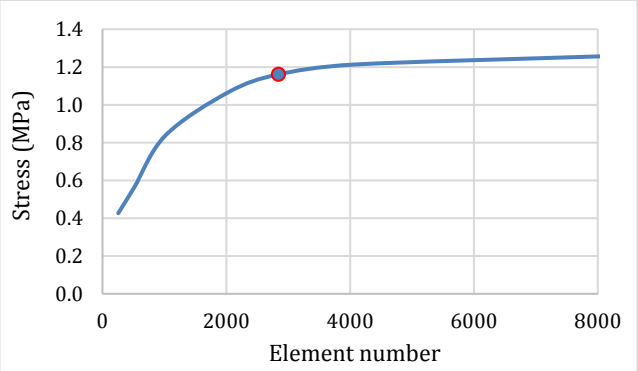

Fig. 8. Evaluation for optimum finite element mesh around upstream face thalweg.

Analyses were conducted using different discretized finite element meshes to observe stress increments resulting from sudden section loss around the gallery. The investigation focused on the dam body, where the number of optimum finite elements was determined based on the results obtained from numerical analyses. The outlined research methodology is depicted in Fig. 8.

4. Dynamic Analysis

Along the height of the dam's upstream face, the principal tensile stresses within the concrete are depicted. Figs. 9 and 10 show that the highest primary stresses drop when the reservoir is empty. Furthermore, when subjected to gravity acceleration, all models exhibit a decrease in maximum tensile stresses. When gravity acceleration is ignored, maximum tensile stresses rise in the full reservoir scenario compared to the empty situation.

5. Performance Analysis

The research investigates the seismic performance of the Akçakoca Roller Compacted Concrete (RCC) Dam, focusing on the impact of gravitational acceleration on its seismic behavior. The study considers both empty and full reservoir conditions, taking into account or neglecting the effects of gravity. Time-history analyses are conducted using the north-south and vertical components of the 1999 Düzce earthquake, as depicted in Figs. 6-7.

The evaluation of demand-capacity ratios, ranging from 1 to 2, is carried out for the primary tensile stresses experienced by the concrete. Figs. 11-14 depict the cycles of major tensile stresses derived from linear time-history analysis under various conditions. In the case of a full reservoir, the major tensile stresses consistently exceed the tensile strength of the concrete, as shown in Fig. 12a, even when the demand-capacity ratio (D/C) is equal to 2. Moreover, the tensile strength of the concrete is recurrently surpassed in the scenario of an empty reservoir. The presence of reservoir water, as indicated in Fig. 14, intensifies the primary tensile stresses.

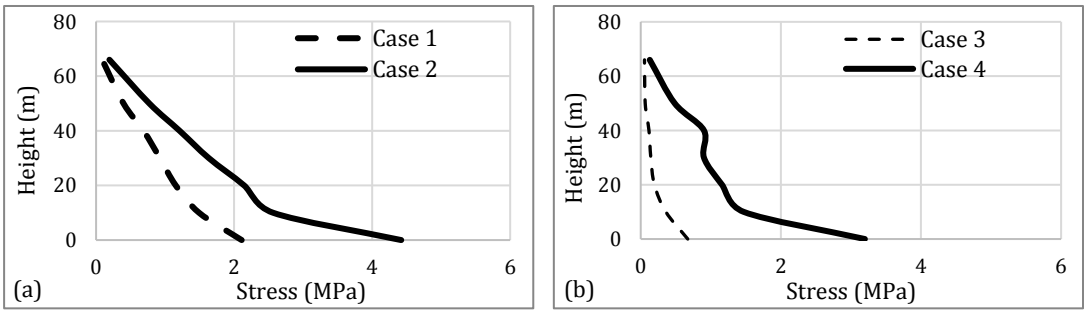

Fig. 9. Maximum principal tensile stress change by height for dam body: (a) Without gravity; (b) With gravity.

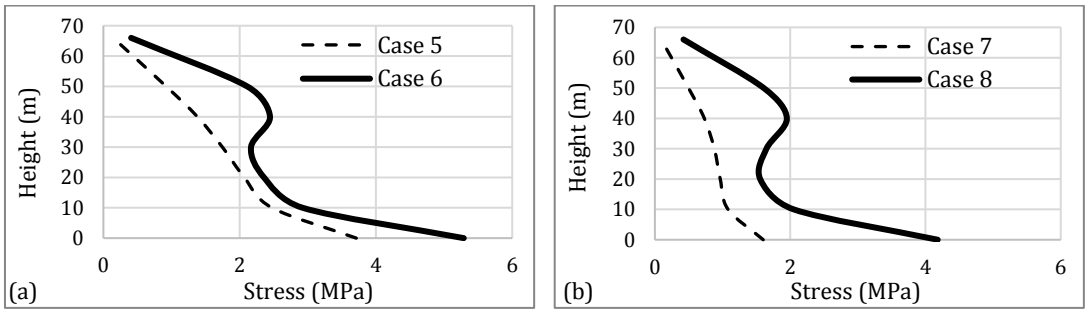

Fig. 10. Maximum principal stress change by height for dam-foundation interaction: (a) Without gravity; (b) With gravity.

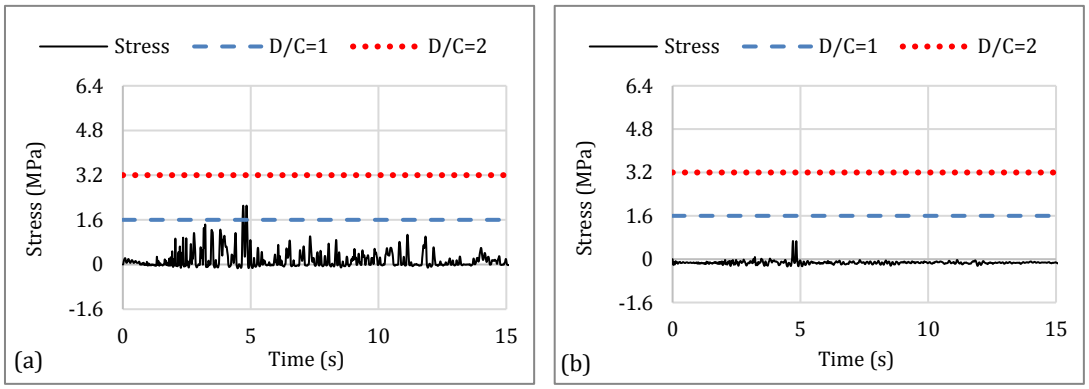

Fig. 11. Maximum principal tensile stress change by time for empty reservoir condition considering dam body: a) Case 1; b) Case 3.

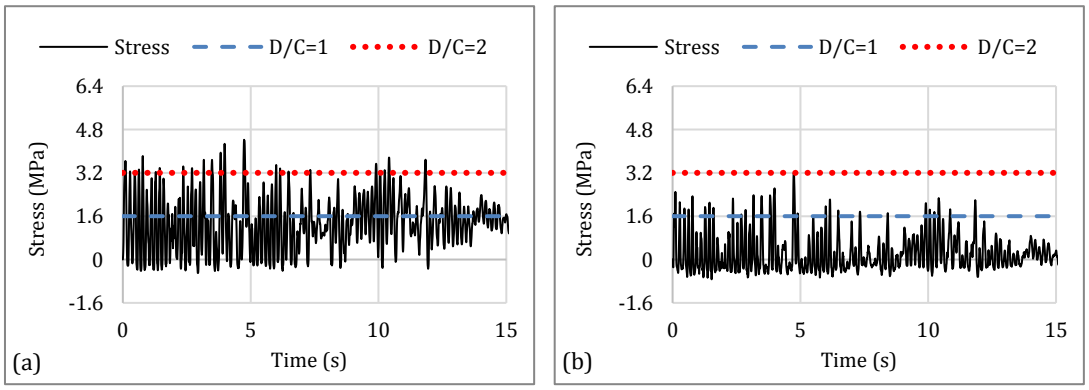

Fig. 12. Maximum principal tensile stress change by time for full reservoir condition considering dam body: a) Case 2; b) Case 4.

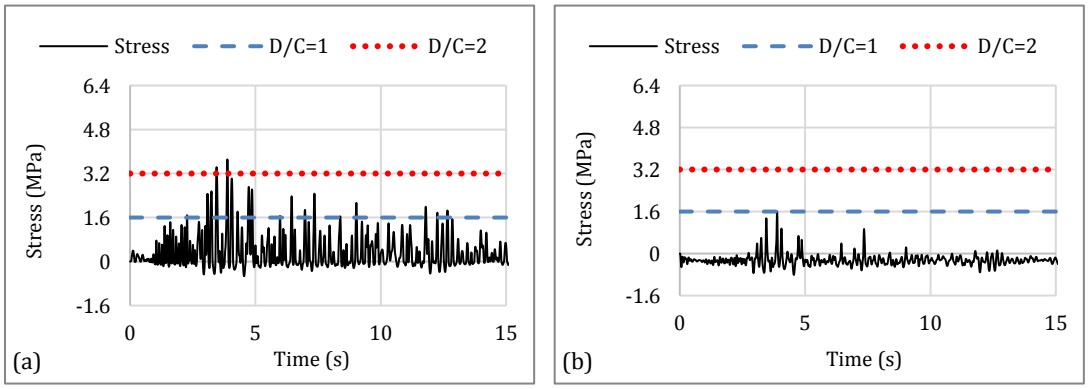

Fig. 13. Maximum principal tensile stress change by time for empty reservoir condition considering dam and foundation rock interaction model: a) Case 5; b) Case 7.

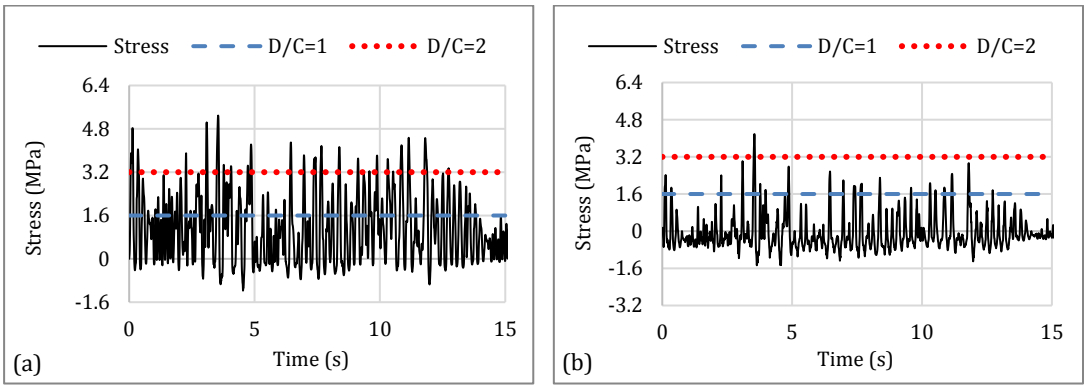

Fig. 14. Maximum principal tensile stress change by time for full reservoir condition considering dam and foundation rock interaction model: (a) Case 6; (b) Case 8.

Performance curves were drawn to determine the earthquake performance of Akçakoca RCC Dam concrete according to linear time history analysis. The earthquake performance of the dam is high when the reservoir is empty and gravity is included. Neglecting the gravitational acceleration reduces the earthquake performance and exceeds the acceptable level in both the empty reservoir case and the full reservoir case. It completely exceeds this level when the reservoir is full and gravitational acceleration is neglected. Analyzes under the influence of full reservoir and gravitational acceleration are given in Figs. 15 and 16. As seen in Fig. 16a, it falls below the accepted curve in the range of 1.3-1.4 in the dam body analysis (Case 4). A similar situation is shown in Fig. 16b. In the case of the dam body and bedrock (Case 8), it falls below the accepted curve in the range of 1.4-1.5. According to linear analysis, damage in the selected point of the concrete seems inevitable since the performance curves are generally above the acceptance curve in both cases.

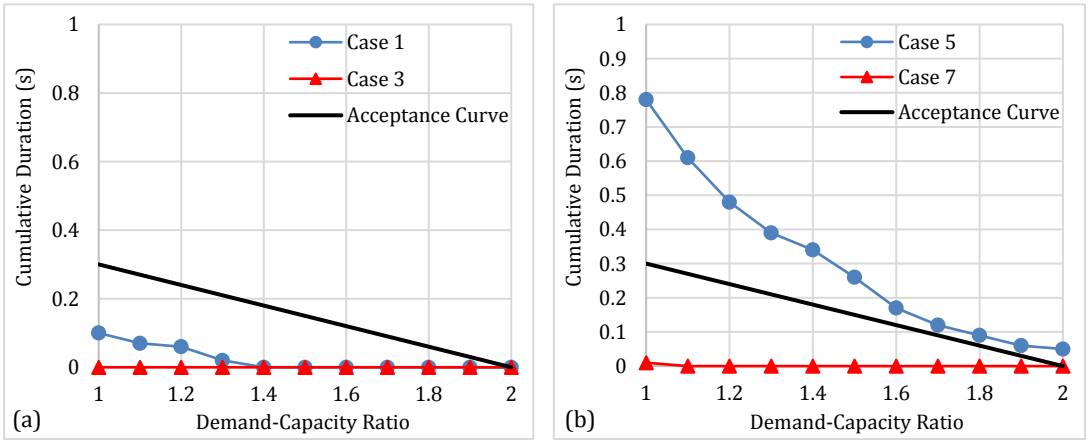

Fig. 15. Performance assessment of empty dam models: a) Only dam body; b) Dam and foundation rock interaction.

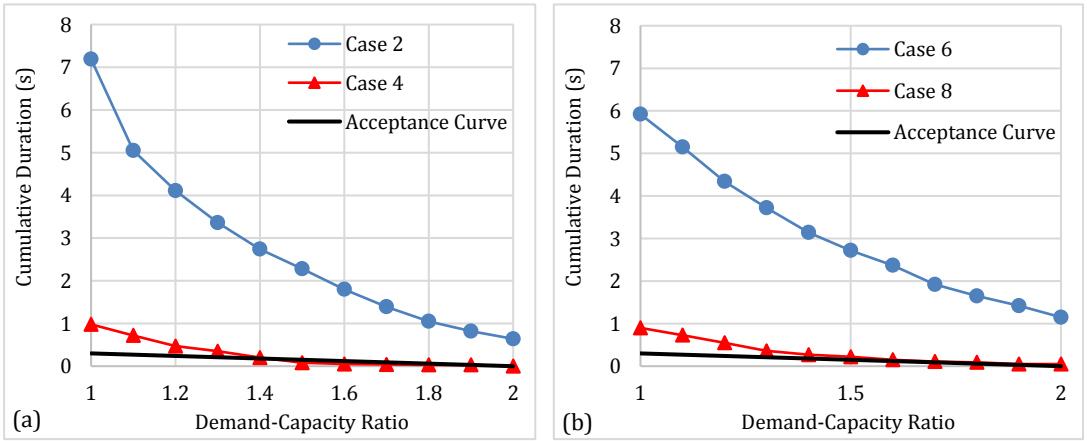

Fig. 16. Performance assessment of full reservoir condition:
a) Only dam body model; b) Dam and foundation rock interaction models.

6. Conclusions

This study explores the seismic behavior and performance of the Akçakoca Roller Compacted Concrete (RCC) Dam through a two-dimensional analysis, considering the interaction between the dam and the reservoir. The representation of reservoir water employs finite elements through the Eulerian-Lagrangian coupled (CEL) approach. Dam models undergo analysis for both horizontal and vertical earthquake components, examining scenarios with and without the influence of gravity.

The numerical analyses clearly demonstrate that the presence of reservoir water significantly influences the earthquake response of the dam. Linear analyses show increased displacements and principal stresses due to hydrodynamic pressure. The earthquake performance assessment of the Akçakoca RCC Dam indicates that substantial damage may occur in the concrete, as revealed by linear time-history analyses in both empty and full reservoir cases. The linear analysis results further demonstrate that the level of damage increases with hydrodynamic pressure. The inclusion or neglect of gravitational acceleration in the analyses leads to notable differences in tensile stresses. In analyses incorporating gravitational force (Cases 3, 4, 7, 8), principal tensile stresses in the dam body are lower for both empty and full reservoir scenarios compared to other analyses (Cases 1, 2, 5, 6). Similar differences are observed in the performance analysis. Under the influence of gravity and in the empty condition, analyses (Cases 3, 7) result in the performance curve falling below an acceptable level, while in other analyses, concrete damage appears inevitable.

Based on the findings of this study, the following suggestions can be clearly outlined:

- It has been observed that gravity effect should be considered as a pre-condition before seismic analyses,
- In assessing the earthquake performance of the RCC dam, it is crucial to model the dam body and foundation rock together.
- Considering hydrodynamic pressure is crucial in earthquake performance analyses to obtain more critical and accurate results.
- Conducting nonlinear analyses is recommended to assess the earthquake performance of an RCC dam more reliably, especially after incorporating the effects of gravity in the analyses.

Acknowledgements

None declared.

Funding

The authors received no financial support for the research, authorship, and/or publication of this manuscript.

Conflict of Interest

The authors declared no potential conflicts of interest with respect to the research, authorship, and/or publication of this manuscript.

Author Contributions

All of the authors made substantial contributions to conception and design, or acquisition of data, or analysis and interpretation of data; were involved in drafting the manuscript or revising it critically for important intellectual content; and gave final approval of the version to be published.

Data Availability

The datasets created and/or analyzed during the current study are not publicly available, but are available from the corresponding author upon reasonable request.

References

ABAQUS (2014). Version 6.14. ABAQUS user's manual, Dassault Systèmes, SIMULIA.

AFAD (2023). Department of Disaster and Emergency, Ministry of Internal Affairs, Türkiye. https://deprem.afad.gov.tr/content/131 [accessed 01-11-2023].

Alebmbagheri M (2016). Earthquake damage estimation of concrete gravity dams using linear analysis and empirical failure criteria. *Soil Dynamics and Earthquake Engineering,* 90, 327–339.

Bathe KJ (1996). Finite Element Procedures. Prentice Hall Upper Saddle River, New Jersey 07458.

Bayraktar A, Kartal ME, Basaga HB (2009). Reservoir water effects on earthquake performance evaluation of Torul concrete-faced rockfill dam. *Water Science and Engineering*, 2(1), 43-57.

Benson DJ (1997). A mixture theory for contact in multi-material Eulerian formulations. *Computer Methods in Applied Mechanics and Engineering*, 140, 59-86.

Benson DJ, Okazawa S (2004). Contact in a multi-material Eulerian finite element formulation. *Computer Methods in Applied Mechanics and Engineering,* 193, 4277-4298.

Calis G, Yıldızel S (2019). Investigation of roller compacted concrete: Literature review. *Challenge Journal of Concrete Research Letters*, 10(3), 63-74.

Cervera M, Oliver J, Prato T (2000). Simulation of construction of RCC dams, I: Temperature and aging. *Journal Structural Engineering,* 126(9), 1053-1061.

Dou SQ, Li JJ, Kang F, (2019). Health diagnosis of concrete dams using hybrid FWA with RBF-based surrogate model. *Water Science and Engineering,* 12(3), 188-195.

DSİ (2023). General Directorate of State Hydraulic Works, Ministry of Agriculture and Forestry, Türkiye. https://dsi.gov.tr/Galeri/ResimGaleriDetay/608 [accessed 01-11-2023].

Erdik M (2000). Report On 1999 Kocaeli and Düzce (Türkiye) Earthquakes. Bogaziçi University-Department of Earthquake Engineering. http://www.koeri.boun.edu.tr/earthqk/earthqk.html [accessed 01-11-2023].

Hariri-Ardebili MA, Seyed-Kolbadi SM, Kianoush MR (2016). FEM-based parametric analysis of a typical gravity dam considering input excitation mechanism. *Soil Dynamics and Earthquake Engineering*, 84, 22–43.

He JP, Jiang ZX, Zhao C, Peng ZQ, Shi YQ (2018). Cloud-Verhulst hybrid prediction model for dam deformation under uncertain conditions. *Water Science and Engineering,* 11(1), 61-67.

Hongwei L, Wang L, Pei L, Chen J, Lu X, Deng D (2023). An advanced method for evaluating the cracking risks of gravity dams during the construction period considering the uncertainty of thermodynamic parameters. *Structures,* 53, 537–549.

Huang J (2018). An incrementation-adaptive multi-transmitting boundary for seismic fracture analysis of concrete gravity dams. *Soil Dynamics and Earthquake Engineering,* 110, 145–158.

Kartal ME, Cavusli M, Sunbul AB (2017). Assessing seismic response of a 2D roller-compacted concrete dam under variable reservoir lengths. *Arabian Journal of Geosciences,* 10: 488.

Kartal ME, Karabulut M (2018). Earthquake performance evaluation of three-dimensional roller compacted concrete dams. *Earthquakes and Structures*, 14(2), 167-178.

Li Z, Wu Z, Chen J, Pei L, Lu X (2021). Fuzzy seismic fragility analysis of gravity dams considering spatial variability of material parameters. *Soil Dynamics and Earthquake Engineering,* 140, 106439.

Li Z, Wang L, Luo Z (2022). A feature-driven robust topology optimization strategy considering movable non-design domain and complex uncertainty. *Computer Methods in Applied Mechanics and Engineering*, 401, 115658.

Liu Y, Wang L, Li M, Wu Z (2022). A distributed dynamic load identification method based on the hierarchical-clustering-oriented radial basis function framework using acceleration signals under convex-fuzzy hybrid uncertainties. *Mechanical Systems and Signal Processing*, 172, 108935.

Luo DN, Hu Y, Li QB (2016). An interfacial layer element for finite element analysis of arch dams. *Engineering Structures,* 128, 400-414.

Sharma V, Fujisawa K, Murakami A (2020). Space–time FEM with block-iterative algorithm for nonlinear dynamic fracture analysis of concrete gravity dam. *Soil Dynamics and Earthquake Engineering,* 131, 105995.

Skrzat A (2012). Application of coupled Eulerian-Lagrangian approach in metal forming simulations. *Zeszyty Naukowe Politechniki Rzeszowskiej*, Nr 284, *Mechanika z*. 84 (4/12).

Subrata M, Damodar M (2014). Experimental investigation on nonlinear dynamic response of concrete gravity dam-reservoir system. *Engineering Structures,* 80, 289–297.

Sunbul AB, Mungan H, Sünbül F, Kartal ME (2018). Investigation of seismic behavior of a clay core rock fill dam using finite element method. *Eurasian Journal of Civil Engineering and Architecture,* 2(1), 7-16.

Wang G, Wang Y, Lu W, Zhou C, Chen M, Yan P (2015). XFEM based seismic potential failure mode analysis of concrete gravity dam–water–foundation systems through incremental dynamic analysis. *Engineering Structures*, 98, 81–94.

Wang L, Zhao Y, Liu J, Zhou Z (2023). Uncertainty-oriented optimal PID control design framework for piezoelectric structures based on subinterval dimension-wise method (SDWM) and non-probabilistic time-dependent reliability (NTDR) analysis. *Journal of Sound and Vibration,* 549, 117588.

Wilson EL, Khalvati M (1983). Finite elements for the dynamic analysis of fluid-solid systems. *International Journal Numerical Methods Engineering,* 19, 1657–1668.

Yang J, Qu XD, Chang M (2019). An intelligent singular value diagnostic method for concrete dam deformation monitoring. *Water Science and Engineering,* 12(3), 205-212.

Yin P, Wang K, Chen L, Zhang Y, Yang K, Wang J (2023) Horizontal Bearing Capacity and Reliability of Piles in Coastal Soft Soil Considering the Time-Varying Characteristics. *Journal of Marine Science and Engineering,* 11(2), 247.

Zhang MX, Li MC, Shen Y, Ren QB, Zhang JR (2019). Multiple mechanical properties prediction of hydraulic concrete in the form of combined damming by experimental data mining. *Construction and Building Materials,* 207, 661-671.